LV-2014-007

Landsvirkjun

Geochemical assessment of the utilization of IDDP#1, Krafla

Report no: LV-2014-007

Landsvirkjun

Geochemical assessment of the utilization of IDDP#1, Krafla

Andri Stefánsson

January 2014

Key Page

Landsvirkjun

LV report no:	LV-2014-007	**Date:**	14.01.2014
Number of pages:	59	**Copies:**	
Distribution:	☐ **On www.lv.is** ☐ **Open** ☐ **Limited until**		
Title:	Geochemical assessment of the utilization of IDDP#1, Krafla		
Authors/Company:	Andri Stefánsson		
Project manager:	Sigurður Hafsteinn Markússon		
Prepared for:	Landsvirkjun hf		
Co operators:			

Abstract: The topic of this report is the geochemistry associated with utilization of IDDP-1 in Krafla. It covers three major aspects: (1) The chemical composition and geochemical processes controlling fluid chemistry in the Krafla system, (2) The chemical composition of superheated vapor discharged by IDDP-1 at Krafla, the formation and the geochemical behavior of superheated vapor as a function of temperature and pressure and (3) The geochemistry associated with reinjection into deeper parts of the Krafla geothermal systems using the IDDP-1 well.

Keywords: IDDP-1, Krafla, geochemistry

ISBN no:

Approved by Landsvirkjun's project manager

Table of Contents

Summary and main conclusions

The topic of this report is the geochemistry associated with utilization of IDDP-1 in Krafla. It covers three major aspects:

- The chemical composition and geochemical processes controlling fluid chemistry in the Krafla system
- The chemical composition of superheated vapor discharged by IDDP-1 at Krafla, the formation and the geochemical behavior of superheated vapor as a function of temperature and pressure
- The geochemistry associated with reinjection into deeper parts of the Krafla geothermal systems using the IDDP-1 well.

The geochemistry of geothermal fluids in Krafla

The chemical composition of geothermal fluids in the Krafla geothermal system were observed to be controlled at close to equilibrium with common secondary minerals found in the system, the equilibrium condition depending on temperature. The elements that are controlled include Si, Na, K, Ca, Mg, Al, Fe, CO_2, H_2S and H_2. Elements that are not incorporated into secondary minerals and show mobile behavior include Cl and B.

The geochemistry and utilization of superheated vapor

Superheated vapor that discharged the IDDP-1 well at Krafla was likely formed upon boiling of geothermal water to single phase vapor at constant temperature and pressure by increased enthalpy. The cause of such increased enthalpy may be high-thermal gradients around magmatic intrusions. Addition of gases by magma degassing may also have contributed to the volatile content of the vapor; however, such direct magma gas input is not necessary to explain the fluid geochemistry within the Krafla system.

The formation process of boiling of geothermal water to single phase vapor leads to quantitative precipitation of non-volatiles (Na, K, Ca, Mg, Al, Fe, SO_4) and partial precipitation of silica, but does not affect concentrations of volatiles (CO_2, H_2S, Cl, F, B). The process may lead to massive silica (quartz) precipitation and reduction of permeability.

The chemical path upon ascent and depressurization of superheated vapor (and supercritical fluid) depend on the initial enthalpy (h) and pressure conditions of the system. If h <2800 kJ/kg (below maximum enthalpy of vapor in a two-phase system), ascent and depressurization of superheated vapor leads to formation of a small fraction of vapor condensate, such condensed vapor (water) being very enriched in Cl, F and B and having a low pH value. If the enthalpy of the superheated vapor is greater than the maximum

enthalpy of vapor in the two-phase field (>2800 kJ/kg) the depressurization occurs in the vapor only stability field.

Depressurization of superheated vapor may lead to severe silica scaling problems due to decrease in silica (quartz) solubility upon depressurization. In the case of IDDP-1 well conditions, the rate of silica scaling could be on the order of ≥150 kg/day SiO_2.

The geochemical aspects of reinjection into geothermal systems

Reinjection of geothermal waste water or non-thermal water into the deeper parts of the Krafla geothermal system using the IDDP-1 well will probably not have major effects on the geochemistry of the system. The reinjection water will react with the basaltic host rock of the system and approach equilibrium conditions of the geothermal fluids under an insignificant degree of reaction (<0.1 mole basalt dissolved per kg of rock). This process is observed to result in secondary mineral formation similar in nature compared to the observed secondary mineralogy within the Krafla system. Mixing of reinjection water with geothermal fluids may further help this process of geochemical homogenization. The equilibrated reinjection water will have a similar composition to the equilibrated geothermal water at Krafla with the exception of a very low CO_2 and H_2S concentration and consequently a slightly higher pH.

The possible geochemical signatures associated with reinjection within production wells may be difficult to assess without using artificial tracers. The use of such tracers in combination with non-reactive elements like Cl is probably the most feasible method for tracing mixing of reinjection fluids with equilibrated geothermal fluids.

Next steps

In relation to geochemistry and hydrogeology, the next step regarding utilization of the IDDP-1 well is to better constrain the process of reinjection. This work would need to include:

- Testing suitable tracers to be used to follow flow paths and mixing trends. Trace amounts of common tracers injected into a geothermal system may show reactive geochemical behavior within porous rocks under geothermal conditions as well as thermal instability. Both are poorly understood. Therefore, it is important to perform tests under controlled conditions, for example in the laboratory, to evaluate the geochemical and thermal behavior of suitable tracers.
- The reinjection water at Krafla is depleted in CO_2 and H_2S compared with the geothermal water in the system. It follows that it could be possible and actually feasible geochemically to add CO_2 and/or H_2S to the reinjection fluid. The geochemical feasibility of such fluid reinjection should be explored as a potential way of reducing chemical emissions (CO_2 and H_2S) to the environment.

- Continuous reinjection may leach out mineral forming elements from the rock, leading to geochemical changes with continuous reinjection over a period of time. The geochemical and hydrological features of such continuous reinjection need to be better explored in order to evaluate the mass and time of possible reinjection.

1 Introduction

The Icelandic Deep Drilling Program (IDDP) started in 2000. The purpose was to investigate the possibility of obtaining fluids at supercritical conditions from active geothermal systems. The first well was IDDP-1, drilled in Krafla in 2008 to 2009. The original target depth was about 4.5 km, but on 7th July 2009, the drilling came to a halt after drilling into molten magma at around 2.1 km depth (Mortensen et al., 2010; Gautason et al., 2010; Hólmgeirsson et al., 2010; Markússon et al., 2013). After a heating up period, the fluids discharging the IDDP-1 well were superheated vapor having temperatures of around 450°C and pressures of 140 bars. The maximum flow was around 45-50 kg/sec and the fluid enthalpy corresponded to 3200 kJ/kg (Markússon et al., 2013).

Severe problems were soon encountered related to the chemistry of the superheated vapor discharging IDDP-1 (Fridriksson et al., 2013; Óskarsson and Fridriksson, 2013). The fluids had very low buffer capacity resulting in acid pH values of the vapor condensates (pH <3). In addition, solid particles were encountered in the vapor eroding the well and wellhead and severe silica formation occurred in the wellhead upon depressurization. Therefore, in order to utilization the superheated vapor for geothermal power production, these chemical problems would need to be overcome. The possible methods of scrubbing and neutralizations as well as silica scaling associated with IDDP-1 are discussed elsewhere (Hauksson and Markússon, 2013a, 2013b).

The other possibility of utilization of IDDP-1 would to use it as a reinjection well. In this way, it could be possible to enhance thermal extraction from reservoir rocks along flow-paths from the IDDP-1 well to nearby production wells.

The purpose of this work was to evaluate the geochemistry associated with utilization of IDDP-1 in Krafla, including:

- Study the geochemical behavior of superheated vapor in relation to utilization of IDDP-1 or similar fluids.
- Assess the geochemical feasibility of reinjection of wastewater or non-thermal groundwater into deeper parts (>2000 m) of the Krafla geothermal system.
- Study the geochemical processes that may occur in the Krafla system upon such reinjection and possible geochemical effects of production well fluids.
- Suggest a possible chemical monitoring scheme in order to evaluate the effects of possible reinjection into IDDP-1 in the Krafla geothermal system.

These issues are accordingly addressed within this report:

- The chemical composition and geochemical processes controlling fluid chemistry within the Krafla system were assessed. This is the geochemical base to which changes are applied upon reinjection.
- The chemical composition and geochemical processes of superheated vapor, i.e. IDDP-1 fluids, were studied, including possible origin and formation of superheated vapor and geochemical behavior as a function of temperature and pressure, in particular in relation to silica formation.
- The chemistry of potential reinjection fluids into the IDDP-1 was studied and their chemical changes upon temperature and pressure increase as well as mixing with geothermal fluids.

2 The geochemistry of geothermal fluids in Krafla

2.1 Sampling and chemical analysis of two-phase well fluids

An overview of the sampling procedure for two-phase (water and vapor) well discharges is shown in Figure 2.1 and a summary of major sample treatment and the analytical method is given in Table 2.1. The sampling and analytical procedures have been described in detail elsewhere (Arnórsson et al., 2006; Stefánsson et al., 2007; Kaaslainen and Stefánsson, 2011). The liquid and vapor phase were separated using a Webre separator that was connected to the wellhead or pipeline going away from the wellhead. For sampling of two-phase well discharges it is crucial to make sure that no condensation occurs upon cooling from the wellhead or well pipe into the separator and out of the separator. This is done by minimizing the metal mass as possible (safety issues need to be fulfilled) in valves, pipes and tubes and insulating all exposed surfaces as possible.

Vapor samples were collected into pre-evacuated gas bulbs (100-250 mL) containing 5-15 mL 50% w/v KOH. In this way, the non-condensable gases are concentrated within the gas-head space of the gas bulb and the condensable gases are concentrated within the alkaline liquid. Non-condensable gases routinely analyzed include H_2, N_2, O_2, Ar, CH_4 and condensable gases routinely analyzed include CO_2 and H_2S. The non-condensable gases were analyzed within the head space of the gas bulbs using Gas Chromatography (GC). The concentrations of CO_2 and H_2S were analyzed within the alkaline condensate using modified alkalinity titration and precipitation titration, respectively.

Liquid phase samples were cooled down using a stainless steel spiral that was connected to the Webre separator in-line. The liquid phase was analyzed for major cations including Si, B, Na, K, Ca, Mg, Fe and Al and major anions including F, Cl and SO_4, as well as for CO_2, H_2S and pH. Samples for major cation determination were filtered through 0.2 µm filters (cellulose acetate) into polypropylene bottles and acidified to 0.5% HNO_3 (Suprapur® Merck) and analyzed using ICP-OES. Samples for major anion and CO_2 determination were also filtered through 0.2 µm filters (cellulose acetate) into polypropylene and amber glass bottles but not further treated, respectively, and analyzed using ion chromatography (IC). pH and H_2S were determined on site in samples that had been cooled down but not filtered. pH was analyzed by pH electrodes and H_2S by precipitation titration.

The quality of the sampling and chemical analysis was ensured using several methods. Firstly, during all chemical analysis, well known standard solutions were used for calibration. Secondly, quality check solutions were run as unknown during chemical analysis to check the performance of the instrument. Thirdly, all sample analyses were made in duplicate. Based on the duplicate analysis the analytical precision was calculated at the 95%

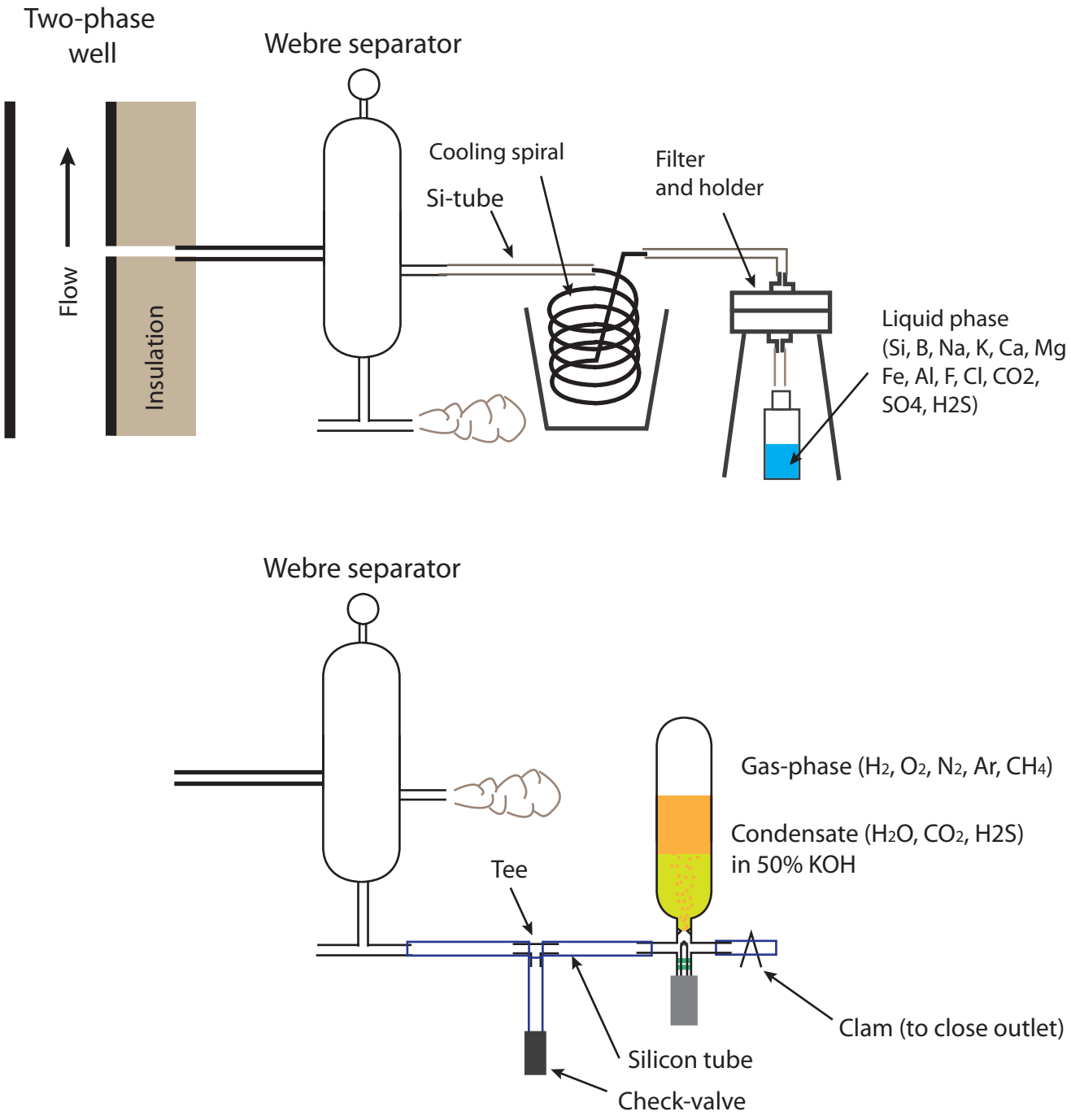

Figure 2.1. Schematic picture of sample configuration for two-phase (liquid and vapor) well discharges.

Table 2.1
Summary of sampling treatment and analytical methods used for liquid and vapor phase samples

Comonent	Sampling method	Analytical method	Standard and control samples [b]
Liquid phase			
pH	cooled, untreated, on-site	pH electrode	com. pH buffers
H_2S	cooled, untreated, on-site	In-site titration	prim. meas.
Si	cooled, filtered (0.2µm), 0.5% HNO_3	ICP-OES	spói05
B	cooled, filtered (0.2µm), 0.5% HNO_3	ICP-OES	spói05
Na	cooled, filtered (0.2µm), 0.5% HNO_3	ICP-OES	spói05
K	cooled, filtered (0.2µm), 0.5% HNO_3	ICP-OES	spói05
Ca	cooled, filtered (0.2µm), 0.5% HNO_3	ICP-OES	spói05
Mg	cooled, filtered (0.2µm), 0.5% HNO_3	ICP-OES	spói05
Fe	cooled, filtered (0.2µm), 0.5% HNO_3	ICP-OES	spói05
Al	cooled, filtered (0.2µm), 0.5% HNO_3	ICP-OES	spói05
Cl	cooled, filtered (0.2µm)	IC	com. standards
SO_4	cooled, filtered (0.2µm)	IC	com. standards
F	cooled, filtered (0.2µm)	IC	com. standards
CO_2	cooled, filtered (0.2µm)	IC	com. standards
Vapor phase			
CO_2	Gas bulb, 5-15 ml 50% KOH	Titration	prim. meas.
H_2S	Gas bulb, 5-15 ml 50% KOH	Titration	prim. meas.
H_2	Gas bulb, 5-15 ml 50% KOH	GC	air and com. standards
CH_4	Gas bulb, 5-15 ml 50% KOH	GC	air and com. standards
N_2	Gas bulb, 5-15 ml 50% KOH	GC	air and com. standards
Ar	Gas bulb, 5-15 ml 50% KOH	GC	air and com. standards
O_2	Gas bulb, 5-15 ml 50% KOH	GC	air and com. standards

[a] If not indicated percent precition at the 95% confidence level.
[b] prim. measurements = primary standard measurements, i.e. no standard needed; spói95 = University of Iceland in-house ICP-OES standard used for geothermal waters, based on comercial certified standards; com. standards = comercial certified standards.

confidence level. Fourthly, when all the chemical analyses had been carried out the ion charge balance was calculated using either or both the WATCH program (Arnórsson et al., 1982; Bjarnason, 1994) and PHREEQC (Pharkhurst and Appelo, 1999). Samples used in this study all showed an ion imbalance of less than 10%. The precision based on duplicate analysis was <5% in most cases

2.2 Chemical composition of two-phase well fluids

The results of the chemical analysis of geothermal well fluid discharges in Krafla collected during 1998 to 2011 are given in Table 2.2. The people involved in the sampling and analyses include: Andri Stefánsson, Jóhann Gunnarsson Robin, Hanna Kaaslainen and Niels Giroud and Ingvi Gunnarsson.

Table 2.2
Krafla geothermal well-fluid samples used in this study to assess the control on fluid composition. All samples were collected and analyzed by reseracher at University of Iceland

Sample #	Location	Well #	Date	p^{sample}	Enthalpy	Liquid phase (ppm)														Steam phase (mmol/kg)						
				bar (g)	kJ/kg	pH / °C	SiO_2	B	Na	K	Ca	Mg	Fe	Al	Cl	F	CO_2	SO_4	H_2S	H_2	N_2	O_2	CH_4	Ar	CO_2	H_2S
04-3009	Hvitholl	K-21	20/10/04	15	1167	8.58 / 17.8	502	0.603	150	19.8	1.188	0.001	0.0035	1.511	72.2	1.017	49.7	67	62.1	5.26	1.08	0	0.24	0.024	96.6	7.2
04-3010	Leirbotnar	K-13	20/10/04	15.5	1941	8.34 / 18.1	432	0.9	244	26.6	4.473	0.002	0.004	1.166	31.8	0.933	67.9	303.9	72.6	46.99	13.12	0	0.117	0.222	157.7	11.9
04-3012	Vesturhlidar	K-34	20/10/04	17.5	2636	7.24 / 19.4	554	0.693	162	30.7	1.181	0.004	0.0137	1.236	99.6	1.341	90.6	44.5	88.9	110.42	7.99	0	0.344	0.175	413	27.6
04-3014	Vitismor-Vesturhlidar	K-32	20/10/04	14.5	1910	8.4 / 19.1	867	1.619	235	53.9	1.558	0.001	0.0022	1.674	147.8	1.38	17.9	167.5	89.5	24.35	1.95	0	0.045	0.042	79.8	24.2
04-3015		K-15	20/10/04	14.5	1499	8.68 / 18	730	1.128	222	39.1	2.059	0.001	0.0012	1.878	36.4	1.271	16	247.9	93.2	11.69	3.22	0	0.055	0.072	58	12.6
04-3019	Sudurhlidar	K-20	21/10/04	11	2543	7.8 / 18.1	859	2.175	259	52.4	1.966	0.002	0.0022	1.072	227	1.272	158	5.8	75.2	41.47	1.97	0	0.333	0.052	437	25.8
04-3021	Sudurhlidar	K-17	21/10/04	28.5	2547	7.88 / 18.9	653	1.359	118	19.8	0.202	0.000	0.0017	1.929	14.9	1.847	69.4	4.7	108.5	32.18	3.62	0	0.628	0.081	165.9	18.9
04-3022	Sudurhlidar	K-16	21/10/04	11	2451	7.36 / 19	662	1.735	194	32.8	0.883	0.002	0.0038	1.026	133.2	2.114	159.3	12.4	61.9	78.27	3.59	0	1.25	0.097	600	32.2
04-3023	Leirbotnar	K-24	21/10/04	2.9	887	9.29 / 16.9	381	0.55	221	17.5	3.585	0.001	0.0027	0.855	45.6	0.825	20.3	241.3	31.7	0.35	3.73	0	0.353	0.091	23.8	3.4
11-KRA-01	Sudurhlidar	K-17	15/10/11	18.0	2399	8.80 / 23.1	641	1.37	129	20.5	0.27	0.009	0.027	1.49	17.9	1.8	83.9	5.4	101.84	22.85	1.61	0.00	0.18	0.03	102.37	24.13
11-KRA-02	Sudurhlidar	K-16A	15/10/11	10.5	2660	7.35 / 23.6	653	2.00	194	31.7	0.85	0.004	0.028	1.06	137.7	1.8	230.1	10.8	72.03	35.12	1.02	0.00	0.33	0.03	481.70	38.96
11-KRA-04	Vitismor-Vesturhlidar	K-32	16/10/11	9.5	1468	9.12 / 18.0	529	0.63	260	40.5	3.06	0.006	0.007	1.46	42.0	1.2	59.8	279.9	103.25	12.62	1.08	0.00	0.08	0.02	56.96	23.48
11-KRA-05	Vesturhlidar	K-33	16/10/11	8.5	2769	8.42 / 19.2	775	2.92	161	28.7	0.75	0.004	0.025	0.43	97.6	1.9	162.3	7.3	120.46	27.04	1.14	0.00	0.03	0.02	75.84	45.59
11-KRA-06	Sudurhlidar	K-20	17/10/11	10.5	2776	8.25 / 17.3	898	3.29	278	49.9	1.54	0.008	0.015	0.22	234.5	1.7	197.1	5.1	96.96	34.67	1.40	0.00	0.17	0.03	389.44	40.41
11-KRA-08	Leirbotnar	K-24	18/10/11	3.4	852	9.59 / 17.7	367	0.60	203	16.5	2.72	0.039	0.012	0.75	44.2	0.8	45.7	222.9	28.36	0.24	3.19	0.00	0.28	0.07	43.91	1.28
11-KRA-09	Leirbotnar	K-13A	18/10/11	8.0	1553	9.08 / 15.2	454	0.99	227	25.2	3.44	0.006	0.016	1.15	38.5	1.1	57.7	262.1	68.61	17.60	1.02	0.00	0.06	0.02	67.55	18.38
11-KRA-10	Hvitholl	K-21	18/10/11	10.0	1058	8.90 / 21.0	513	0.74	173	23.0	1.33	0.002	<0,010	1.33	134.7	0.9	54.0	54.7	42.00	6.54	2.94	0.00	0.85	0.06	67.65	11.74
11-KRA-11	Leirbotnar	K-5	19/10/11	3.4	998	9.22 / 15.7	351	0.59	203	17.8	3.05	0.024	0.012	0.85	41.4	1.0	51.1	218.3	27.61	1.07	2.92	0.00	0.20	0.06	20.31	5.16
11-KRA-12	Leirbotnar	K-27	19/10/11	11.5	1370	9.25 / 14.6	455	0.59	206	27.2	2.61	0.017	0.181	1.46	38.0	1.0	57.2	251.9	42.81	3.24	2.85	0.00	0.25	0.05	43.17	6.86
11-KRA-16	Vitismor-Vesturhlidar	K-40	20/10/11	11.0	2774	6.49 / 9.4	520	2.83	85	15.1	2.11	0.049	0.024	1.45	20.7	1.6	925.8	19.9	32.81	8.70	26.71	0.23	0.12	0.35	473.31	30.38
11-KRA-17	Vesturhlidar	K-34	20/10/11	17.5	2763	7.27 / 9.0	592	5.00	176	30.4	1.72	0.008	0.030	0.95	157.0	1.5	69.8	52.2	63.00	25.10	1.34	0.00	0.06	0.03	246.48	53.87
97-3098	Hvitholl	K-21	25/10/97	18.5	1739	8.71 / 20.6	545	0.68	143	19.9	1.20	0.007	0.022	1.46	57.1	0.97	35.2	69.2	66.5	14.3	0.61	0.003	0.46		110	19.4
97-3099		K-14	25/10/97	8.5	2267	8.78 / 19.5	560	2.57	157	20.7	1.20	0.005	0.015	1.13	35.5	1.73	132.5	45.2	43.0	31.1	1.82	0.039	0.175	0.039	317	32
97-3102	Leirbotnar	K-13	26/10/97	13.2	1551	8.6 / 20.8	443	1.05	280	31.3	6.01	0.005	0.021	1.16	15.2	0.85	51.0	448.6	62.4	20.5	0.97	0.021	0.081	0.021	228	27.2
97-3103		K-28	26/10/97	6.5	1015	9.75 / 20.9	480	0.50	222	25.8	4.01	0.002	0.008	1.05	17.4	0.91	30.8	287.2	36.8	1	33.62	3.646	0.414	0.429	64	2.5
97-3104		K-15	26/10/97	11.7	1790	8.99 / 19.2	797	1.95	206	38.3	1.60	0.005	0.012	2.02	24.5	1.58	43.6	198.9	82.8	21.2	1.88	0.034	0.044	0.034	250	37.5
98-3201	Hvitholl	K-21	23/06/98	14.9	1698	8.88 / 24.6	543	0.62	143	19.2	0.40	0.005	0.037	1.38	74.8	0.97	25.1	134.5	25.2	15.9	22.47	0	4.269	0.367	178	29
98-3205	Leirbotnar	K-5	24/06/98	2.2	1038	9.67 / 23.3	368	0.54	195	18.0	4.41	0.010	0.006	0.86	28.4	0.99	29.9	261.3	33.1	4.4	11.94	0	1.257	0.281	66	6.2
98-3207	Leirbotnar	K-13	24/06/98	11.5	1658	8.16 / 23.6	412	1.06	274	30.1	5.21	0.002	0.006	1.03	22.0	0.74	69.1	524.5	64.8	29.4	3.38	0.073	0.087	0.073	204	25
98-3208	Leirbotnar	K-24	25/06/98	2.3	938	9.73 / 24.2	363	0.49	218	17.2	3.61	0.000	0.003	0.84	30.5	0.76	18.0	316.1	29.0	0.2	9.51	0.232	1.064	0.232	59	7.4

The chemical composition of the two-phase well fluids given in Table 2.2 provides the bases for the assessment of geochemical processes controlling the fluid composition within the Krafla system.

2.3 Calculation of aquifer fluid composition

The calculation of aquifer fluid composition from data on two-phase well discharges (vapor and water) collected at the surface essentially involved two steps, firstly the selection of aquifer reference temperature and secondly the calculation of the aquifer fluid composition and species distribution using an appropriate model.

There are two ways to estimate the temperature beyond the zone of boiling: one is to use geothermometers and the other is to use measured down hole temperatures in thermally stabilized wells at the depth of permeable horizons. Wells may receive water from more than one aquifer, in which case the discharge is mixed. If the producing aquifers have significantly different temperatures, clearly reconstruction of a single aquifer fluid is not valid. Therefore, it is important to study both the depth level of possible aquifers and their respective temperature measurements as well as geothermometry temperatures that are based on local equilibrium between secondary minerals and the fluids.

In the present work the aquifer temperatures were evaluated and selected based on silica geothermometer temperatures that were based on local equilibrium between the fluid and quartz (qtz), according to the reaction:

$$qtz + 2H_2O = H_4SiO_4(aq)$$

For quartz the equilibrium constant was selected from Gunnarsson and Arnórsson (2000).

Aquifers of volcanic geothermal systems penetrated by drill holes may be sub-boiling, i.e. liquid water is only present in the reservoir. In this case, the depth level of first boiling is within the well, at least during the early stages of well discharge when reservoir pressure drawdown is limited, and the system can be approximated as an isolated system. It follows that the aquifer fluid composition may be calculated from:

$$m_i^{d,t} = m_i^{f,t} = m_i^{d,v} x^{d,v} + m_i^{d,l}(1 - x^{d,v})$$

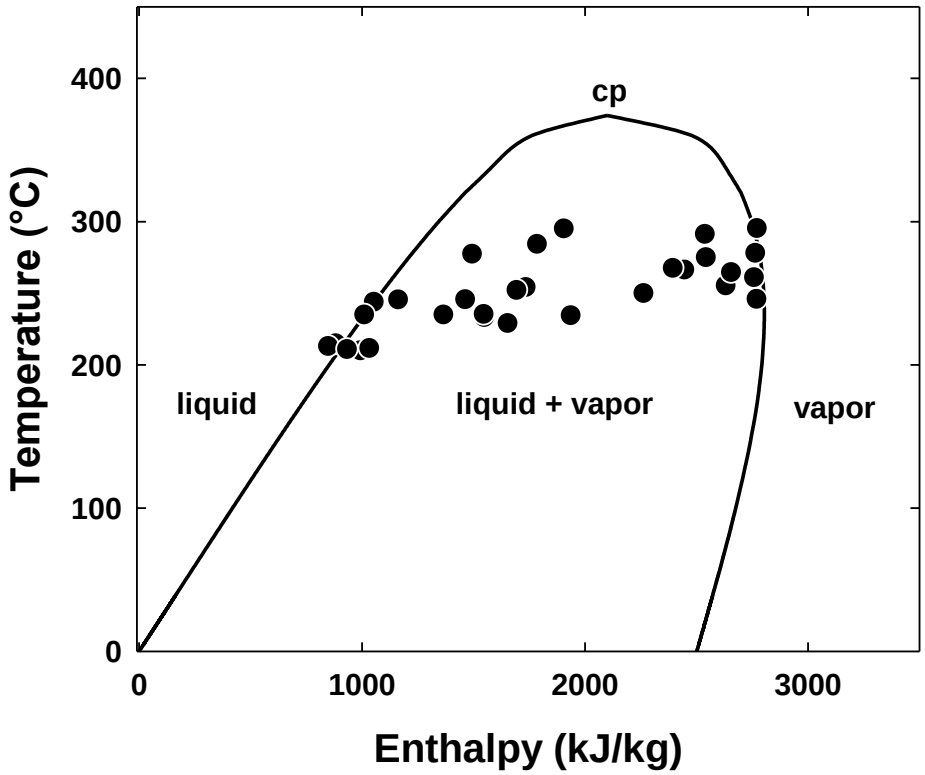

Figure 2.2. *The relationship between temperature and enthalpy for the system H_2O. The curve defines the stability field of liquid only, coexisting liquid and vapor, and vapor only. The symbols are the results of the aquifer temperatures calculated assuming quartz equilibrium and measured discharge enthalpy. As observed, many well discharges express higher enthalpy than could be expected from liquid only in the aquifer. This suggests that vapor is present.*

where $m_i^{d,t}$ and $m_i^{f,t}$ represent the concentration of the i-th component in the aquifer fluid and total discharge, respectively, $m_i^{d,v}$ and $m_i^{d,l}$ the concentration in the vapor and liquid phases discharged at the surface, and $x^{d,v}$ is the vapor fraction at surface. However, wells may intersect an aquifer that is two-phase (steam and water), either because this was the natural state of the reservoir or because reservoir drawdown has led to depressurization boiling within an aquifer. Under these conditions the system aquifer wellhead may still act as if isolated. It is not common, however, that discharge enthalpy is higher than that of the aquifer fluid enthalpy beyond the zone of boiling. Depending on the relative permeability effect, depressurization boiling in the aquifer may lead to phase segregation and hence cause increased enthalpy of the discharge well fluids.

Many well discharges at Krafla were observed to have excess enthalpy (Figure 2.2). In this case, the process of excess vapor at surface has to be taken into account when modelling the aquifer fluid composition. Here the excess enthalpy was assumed to be

caused by the vapor fraction in the aquifer. The physical vapor fraction in the aquifer is defined according to:

$$X^{f,v} = \frac{h^{f,t} - h^{f,l}}{L^f}$$

where $X^{f,v}$ is the initial vapor fraction in the aquifer fluid, $h^{f,t}$ is the total enthalpy of the aquifer fluid, $h^{f,l}$ is the enthalpy of liquid water in the aquifer fluid and L^f is the latent heat of evaporation. In order to obtain $X^{f,v}$, $h^{f,l}$ was assumed to be equal to the measured discharge enthalpy at the surface and $h^{f,l}$ was calculated based on the properties of water at the aquifer temperature. Here this procedure is referred to as model 2. Alternatively, the excess enthalpy was ignored and the total enthalpy of the aquifer fluid was taken to be equal to the enthalpy of liquid water at the aquifer temperature; hence aquifer steam was ignored. In this report this procedure is referred to as model 1.

The calculation of aquifer fluid composition from data on vapor and water collected at the surface was carried out with the aid of the WATCH program (Arnórsson et al., 1982; Bjarnason, 1994).

Alternatively, the process considered to be responsible for the excess steam fraction at the surface may be phase segregation, i.e. a fraction of the liquid water in the aquifer was immobilized by its adhesion to mineral grain surfaces or addition of heat (energy) to the system and enhanced boiling (Arnórsson et al., 2007, 2010; Stefánsson et al., 2011; Scott et al., 2013).

2.4 Aquifer fluid composition

The calculated aquifer fluid composition of a single liquid phase reservoir system (model 1) and of a two-phase reservoir system (model 2) are listed in Tables 2.3 and 2.4, respectively. Model 1 refers to a liquid only reservoir assuming the reservoir enthalpy to be equal to the enthalpy of liquid only water at the reservoir temperature. Model 2 refers to a liquid only reservoir in case of low enthalpy (liquid only enthalpy) well discharges and two-phase reservoirs, liquid and vapor, in case of excess enthalpy well discharges. The reservoir vapor fraction was calculated from the quartz geothermometry temperature and measured enthalpy of the well discharge.

The two models are in reasonable agreement with respect to non-volatile components in all cases except when fluids approached dry steam. The non-volatile

Table 2.3
Aquifer fluid composition at Krafla calculated from model 1. Units are in ppm

Sample #	t^{quartz}	pH_T	SiO2	B	Na	K	Mg	Ca	Al	Fe	F	Cl	SO_4	CO_2	H_2S	H_2	CH_4	N_2
04-3009	245	6.89	446	0.54	133	17.6	0.001	1.06	1.34	0.003	0.90	64.2	60	516	82	1.18	0.43	3.35
04-3010	234	6.75	397	0.83	224	24.46	0.002	4.11	1.07	0.004	0.86	29.2	279	621	99	7.64	0.15	29.59
04-3012	255	6.41	487	0.61	143	27.01	0.004	1.04	1.09	0.012	1.18	87.6	39.2	2262	191	26.78	0.66	26.87
04-3014	294	7.02	655	1.22	178	40.75	0.001	1.18	1.27	0.002	1.04	112	127	871	269	12.00	0.18	13.33
04-3015	277	7.11	587	0.91	179	31.45	0.001	1.66	1.51	0.001	1.02	29.3	199	513	159	4.62	0.17	17.65
04-3019	291	6.68	639	1.62	193	38.98	0.001	1.46	0.80	0.002	0.95	169	4.31	5042	281	21.45	1.37	14.13
04-3021	274	7.09	576	1.20	104	17.48	0.000	0.18	1.70	0.002	1.63	13.2	4.15	918	171	7.63	1.18	11.90
04-3022	266	6.32	536	1.40	157	26.53	0.002	0.71	0.83	0.003	1.71	107.8	10.0	5173	260	30.20	3.83	19.21
04-3023	214	6.87	318	0.46	184	14.59	0.001	2.99	0.71	0.002	0.69	38.0	201	191	46	0.12	0.94	17.36
11-KRA-01	267	7.13	546	1.17	110	17.45	0.008	0.23	1.27	0.023	1.53	15.2	4.60	742	209	6.86	0.42	6.70
11-KRA-02	264	6.49	529	1.62	157	25.66	0.003	0.69	0.86	0.023	1.46	111	8.74	4226	311	13.49	1.01	5.44
11-KRA-04	245	6.97	448	0.53	220	34.32	0.005	2.59	1.24	0.006	1.02	35.6	237	433	210	3.88	0.19	4.61
11-KRA-05	277	7.03	588	2.22	122	21.79	0.003	0.57	0.33	0.019	1.44	74.1	5.54	927	466	13.12	0.13	7.65
11-KRA-06	295	6.84	655	2.40	203	36.4	0.006	1.12	0.16	0.011	1.24	171	3.72	4781	443	18.91	0.74	10.63
11-KRA-08	212	6.97	311	0.51	172	13.99	0.033	2.31	0.64	0.010	0.68	37.5	189	333	31	0.07	0.69	13.63
11-KRA-09	233	6.78	392	0.85	196	21.74	0.005	2.97	0.99	0.014	0.95	33.2	226	457	145	4.87	0.14	3.93
11-KRA-10	243	6.86	439	0.63	148	19.69	0.002	1.14	1.14	0.009	0.77	115	46.8	475	94	1.90	1.97	11.86
11-KRA-11	209	6.97	300	0.50	173	15.2	0.020	2.60	0.73	0.010	0.85	35.4	186	174	49	0.32	0.48	11.96
11-KRA-12	234	7.17	405	0.52	183	24.19	0.015	2.32	1.30	0.161	0.89	33.8	224	261	64	0.72	0.45	8.84
11-KRA-16	245	6.68	447	2.43	73	12.97	0.042	1.81	1.25	0.021	1.38	17.8	17.1	3728	174	2.47	0.27	105.34
11-KRA-17	260	6.33	512	4.33	152	26.31	0.007	1.49	0.82	0.026	1.30	136	45.2	1521	302	6.81	0.13	5.07
97-3098	253	6.86	484	0.60	127	17.69	0.006	1.07	1.30	0.020	0.86	50.8	61.5	569	133	3.21	0.82	1.90
97-3099	249	6.44	464	2.13	130	17.14	0.004	0.99	0.94	0.012	1.43	29.4	37.4	2506	223	10.79	0.48	8.76
97-3102	235	6.45	399	0.95	252	23.62	0.005	5.42	1.05	0.019	0.77	13.7	404	1035	148	4.08	0.13	2.68
97-3103	234	7.18	405	0.42	187	21.75	0.002	3.38	0.89	0.007	0.77	14.7	242	469	44	0.32	1.04	147.98
97-3104	284	6.74	612	1.50	158	29.4	0.004	1.23	1.55	0.009	1.21	18.8	153	2590	360	9.95	0.16	12.23
98-3201	251	6.45	473	0.54	125	16.74	0.004	0.35	1.20	0.032	0.85	65.2	117	1026	149	4.12	8.77	80.65
98-3205	211	6.68	304	0.45	161	14.85	0.008	3.64	0.71	0.005	0.82	23.4	216	533	64	1.56	3.53	58.52
98-3207	228	6.44	372	0.96	248	27.2	0.002	4.71	0.93	0.005	0.67	19.9	474	929	141	5.73	0.13	9.13
98-3208	210	6.70	301	0.41	181	14.26	0.000	2.99	0.70	0.003	0.63	25.3	262	459	67	0.07	2.92	45.53

Table 2.4
Aquifer fluid composition at Krafla calculated from model 2. Units are in ppm

Sample #	t^{quartz}	Liquid Phase														Vapor phase				
		pH_T	SiO_2	B	Na	K	Mg	Ca	Al	Fe	F	Cl	SO_4	CO_2	H_2S	CO_2	H_2S	H_2	CH_4	N_2
04-3009	243	7.52	449	0.54	134	17.71	0.001	1.06	1.35	0.0031	0.91	65	59.9	120	49	9458	697	26	9.33	74
04-3010	229	7.66	400	0.83	226	24.60	0.002	4.14	1.08	0.0037	0.86	29	281.1	105	43	7372	455	101	2.00	392
04-3012	250	7.35	477	0.60	139	26.43	0.003	1.02	1.06	0.0118	1.15	86	38.3	222	53	18429	957	226	5.60	227
04-3014	294	7.62	665	1.24	180	41.32	0.001	1.19	1.28	0.0017	1.06	113	128.4	125	100	4521	1054	65	0.95	72
04-3015	274	7.67	592	0.91	180	31.70	0.001	1.67	1.52	0.001	1.03	30	201.0	91	76	4340	788	43	1.59	164
04-3019	333	7.99	979	2.48	295	59.74	0.002	2.24	1.22	0.0025	1.45	259	6.6	1227	153	18799	857	82	5.24	54
04-3021	277	7.81	609	1.27	110	18.46		0.19	1.80	0.0016	1.72	14	4.4	176	76	7370	656	66	10.19	103
04-3022	261	7.34	523	1.37	153	25.92	0.002	0.7	0.81	0.003	1.67	105	9.8	387	66	27793	1153	167	21.14	106
04-3023	214	6.87	318	0.46	184	14.59	0.001	2.99	0.71	0.0023	0.69	38	201.2	191	46					
11-KRA-01	263	7.85	553	1.18	111	17.67	0.008	0.23	1.28	0.0233	1.55	15	4.7	101	109	4693	852	48	2.94	47
11-KRA-02	248	7.44	470	1.44	140	22.83	0.003	0.61	0.76	0.0202	1.30	99	7.8	273	86	21718	1358	73	5.43	29
11-KRA-04	240	7.73	452	0.54	222	34.61	0.005	2.61	1.25	0.006	1.03	36	239.2	60	117	3610	1071	37	1.84	44
11-KRA-08	212	6.97	311	0.51	172	13.99	0.033	2.31	0.64	0.0102	0.68	37	188.9	333	31					
11-KRA-09	227	7.69	394	0.86	197	21.85	0.005	2.98	1.00	0.0139	0.95	33	227.3	55	75	3819	773	46	1.31	37
11-KRA-10	243	6.97	439	0.63	148	19.7	0.002	1.14	1.14	0.0086	0.77	115	46.8	347	86	39618	2596	398	409	2703
11-KRA-11	204	7.75	303	0.51	175	15.37	0.021	2.63	0.73	0.0104	0.86	36	188.5	39	35	2675	355	6	9.47	237
11-KRA-12	228	7.88	410	0.53	186	24.53	0.015	2.35	1.32	0.1632	0.90	34	227.1	51	43	2589	302	9	5.51	108
11-KRA-16	192	7.57	250	1.36	41	7.27	0.024	1.02	0.70	0.0116	0.77	10	9.6	198	62	20896	1038	18	1.95	750
11-KRA-17	241	7.06	433	3.65	129	22.22	0.006	1.26	0.69	0.0219	1.10	115	38.2	97	66	10913	1847	51	0.95	38
97-3098	251	7.59	488	0.61	128	17.80	0.006	1.07	1.31	0.0197	0.87	51	61.9	83	63	5590	770	34	8.62	20
97-3099	243	7.49	452	2.07	127	16.70	0.004	0.97	0.91	0.0121	1.40	29	36.5	188	78	15105	1164	68	3.04	55
97-3102	232	7.36	400	0.95	253	23.68	0.005	5.43	1.05	0.019	0.77	14	405.4	122	62	12056	1118	50	1.58	33
97-3103	233	7.38	406	0.42	188	21.80	0.002	3.39	0.89	0.0068	0.77	15	242.7	321	41	31245	732	53	175	26278
97-3104	282	7.48	616	1.51	159	29.59	0.004	1.24	1.56	0.0093	1.22	19	153.7	319	130	15044	1688	60	0.99	74
98-3201	250	0.01	474	0.54	125	16.76	0.004	0.35	1.20	0.0323	0.85	65	117.4	107	56	9474	1153	39	84	772
98-3205	206	7.70	307	0.45	162	14.99	0.008	3.67	0.72	0.005	0.83	24	217.6	99	41	7401	452	25	57	942
98-3207	225	7.43	373	0.96	248	27.24	0.002	4.72	0.93	0.0054	0.67	20	474.7	105	60	10319	985	69	1.61	109
98-3208	208	7.44	303	0.41	182	14.34		3.01	0.70	0.0025	0.63	25	263.5	125	48	14116	883	3	117	1832

components include SiO_2, B, Na, K, Ca, Mg, Al, Fe, F, Cl and SO_4. The differences between the models rely on the calculation of volatile components including CO_2, H_2S, H_2, N_2 and CH_4 under excess enthalpy conditions. For model 1, the concentrations of volatiles in the reservoir liquid phase is greater compared to model 2, whereas the volatiles are concentrated in the reservoir vapor phase for model 2.

2.5 Aqueous speciation and mineral saturation state

The aqueous speciation, gas pressures and mineral saturation states were calculated for reservoir fluids, for both model 1 and 2. The calculations were carried out using the PHREEQC program (Parkhurst and Appelo, 1999).

The mineral saturation indices were calculated from the respective reaction quotients and equilibrium constants. The minerals considered were those commonly observed within the Krafla system and similar high-temperature geothermal systems in Iceland including quartz, chlorite, epidote, prehnite, grossularite, wollastonite, albite, microline, zeolites (wairakite), calcite, magnetite, pyrite, pyrrhotite, sulfur and anhydrite (Mortensen et al., 2009). The minerals, mineral reactions and solubility constants are given in Table 2.5. They are based on thermodynamic values from Supcrt92 slop07.dat (Johnson et al., 1992), Gunnarsson and Arnórsson (2000), Benezeth et al. (2001), Ziemniek et al. (1995), Hill (1990), Diakonov et al. (1999) and Marshall and Franck (1981), Holland and Powell (1998), Robie and Hemingway (1995), Neuhoff (2000), Arnórsson and Stefánsson (1999) and Fridriksson (2001). A summary of the stability constants can be obtained in Stefánsson et al. (2009).

The reaction quotients (Q) for the mineral reactions considered are given by

$$Q = \prod a_i^{v_i}$$

where a_i is the activity of the i-th mineral or aqueous species and v_i is its reaction stoichiometry, positive for products and negative for reactants. When the mineral dissolution or precipitation reactions are written with the minerals to the left (reactant), negative saturation indices indicate undersaturation and that the respective mineral is unstable or has the tendency to dissolve if present in the system, whereas zero and positive saturation indices indicate saturation and supersaturation, respectively, and that the minerals are stable and have the potential of precipitating.

Table 2.5
Minerals included in the geochemical model calculations at 100-350°C andwater vapor saturation pressure (p_{sat})

Mineral	Symbol	Chemical composition	Reaction	$\log K(T, p_{sat}) = a + bT + c/T + dT^2 + e\log T$				
				a	b	c	d	e
Quartz	qtz	SiO_2	$qtz + 2H_2O = H_4SiO_4$	-57.502	-0.0106	747	-1.5087E-06	22.110
Clinochlore	chl	$Mg_5Al_2Si_3O_{10}(OH)_8$	$chl + 2H_2O + 8H^+ = 5Mg^{2+} + 2Al(OH)_4^- + 3H_4SiO_4$	340.576	0.4436	11208	-2.9070E-04	-190.728
Daphnite	dap	$Fe_5Al_2Si_3O_{10}(OH)_8$	$dap + 2H_2O + 8H^+ = 5Fe^{2+} + 2Al(OH)_4^- + 3H_4SiO_4$	617.002	0.5540	-858	-3.3601E-04	-303.745
Epidote	epi	$Ca_2Al_2FeSi_3O_{12}(OH)$	$epi + 11H_2O + H^+ = 2Ca^{2+} + Fe(OH)_4^- + 2Al(OH)_4^- + 3H_4SiO_4$	1224.738	0.7588	-28064	-3.9694E-04	-547.838
Clinozoesite	czo	$Ca_2Al_3Si_3O_{12}(OH)$	$czo + 11H_2O + H^+ = 2Ca^{2+} + 3Al(OH)_4^- + 3H_4SiO_4$	1997.556	1.1660	-43990	-5.9048E-04	-878.248
Prehnite	pre	$Ca_2Al_2Si_3O_{10}(OH)_2$	$pre + 8H_2O + 2H^+ = 2Ca^{2+} + 2Al(OH)_4^- + 3H_4SiO_4$	1232.731	0.7607	-24606	-3.9792E-04	-547.640
Grossular	gro	$Ca_3Al_2Si_3O_{12}$	$gro + 8H_2O + 4H^+ = 3Ca^{2+} + 2Al(OH)_4^- + 3H_4SiO_4$	1221.164	0.7654	-18850	-4.0685E-04	-544.150
Wollastonite	wo	$CaSiO_3$	$wo + H_2O + 2H^+ = Ca^{2+} + H_4SiO_4$	-91.644	-0.0116	7418	-7.9588E-06	34.062
Low-albite	alb	$NaAlSi_3O_8$	$alb + 8H_2O = Na^+ + Al(OH)_4^- + 3H_4SiO_4$	635.486	0.4058	-16702	-2.1245E-04	-283.590
Microcline	mic	$KAlSi_3O_8$	$mic + 8H_2O = K^+ + Al(OH)_4^- + 3H_4SiO_4$	636.075	0.3988	-18303	-2.0902E-04	-282.044
Wairakite	wai	$CaAl_2Si_4O_{12}{\cdot}2H_2O$	$wai + 10H_2O = Ca^{2+} + 2Al(OH)_4^- + 4H_4SiO_4$	1319.746	0.8032	-32964	-4.1490E-04	-584.035
Calcite	cc	$CaCO_3(s)$	$cc + H^+ = Ca^{2+} + HCO_3^-$	853.061	0.4131	-18773	-1.8914E-04	-361.511
Magnetite	mt	Fe_3O_4	$mt + 4H_2O = Fe^{2+} + 2Fe(OH)_4^-$	-137.203	-0.0383	102	8.9963E-06	46.959
Pyrite	py	FeS_2	$py + 2H^+ + H_2(aq) = Fe^{2+} + 2H_2S(aq)$	-169.899	-0.0473	4844	1.0275E-05	67.777
Pyrrhotite	pyrr	FeS	$pyrr + 2H^+ = Fe^{2+} + H_2S(aq)$	-283.060	-0.1012	9192	3.4229E-05	114.180
Sulfur	S	S	$S + H_2(aq) = H_2S(aq)$	54.872	0.0248	502	-1.2128E-05	-22.174
Anhydrite	anh	$CaSO_4$	$anh = Ca^{2+} + SO_4^{2-}$	1804.919	0.8489	-42491	-3.8096E-04	-762.156

Table 2.6
Mineral buffer reactions included in the geochemical model calculations at 100-350°C andwater vapor saturation pressure (p_{sat})

Species or spec	Reaction	$\log K(T, p_{sat}) = a + bT + c/T + dT^2 + e\log T + f/T^2$					
		a	b	c	d	e	f
H_2S(aq)	⅓py + ⅓pyrr + ⅔pre + ⅔H_2O = ⅔epi + H_2S(aq)	13.608	-0.04355	-9346.70	2.916E-05	5.139	592324
H_2S(aq)	⅔gro + ⅓py + ⅓pyrr + ⅔qtz + 1⅓H_2O = ⅔epi + ⅔wo + H_2S(aq)	15.343	-0.05095	-9778.80	3.454E-05	5.677	592444
H_2S(aq)	2gro + ¼py + ½mt + 2qtz + 2H_2O = 2epi + 2wo + H_2S(aq)	-0.836	0.00852	-2847.30	-2.366E-06	0.152	-216659
H_2S(aq)	¼py + ½pyrr + 2H_2O = ¼mt + H_2S(aq)	13.589	-0.04488	-9024.50	2.978E-05	5.068	590215
H_2(aq)	4/3pyrr + ⅔pre + ⅔H_2O = ⅔epi + ⅔py + 3H_2(aq)	-1.643	-0.00042	-802.06	7.574E-06	-0.560	-110535
H_2(aq)	⅔gro + 1⅓pyrr + ⅔qtz + 1⅓H_2O = ⅔epi + ⅔wo + ⅔py + H_2(aq)	-1.623	-0.00104	-672.91	8.403E-06	-0.581	-145793
H_2(aq)	6gro + 2mt + 6qtz + 4H_2O = 6epi + 6wo + H_2(aq)	20.211	-0.07295	-10846.00	5.694E-05	7.145	320763
H_2(aq)	pyrr + H_2O = ¾py + ¼mt + H_2(aq)	-1.572	-0.00303	-232.45	9.517E-06	-0.652	-1668874
CO_2(aq)	czo + cc + 1⅓qtz + H_2O = 1⅓pre + CO_2(aq)	-0.860	0.00419	-1710.60	2.683E-06	-0.060	7252
CO_2(aq)	czo + cc+ ⅗qtz = ⅗gro + ⅕H_2O + CO_2(aq)	0.731	0.00114	-3617.40	4.507E-06	0.669	153276
H_4SiO_4	qtz + 2H_2O = H_4SiO_4	-57.502	-0.01060	746.70	-1.509E-06	22.110	
Na^+/K^+	alb + K^+ = Na^+ + mic	-0.589	0.00700	1600.60	-3.430E-06	-1.546	
$Ca^{2+}/(H^+)^2$	1.5pre+2H^+ = 1.5qtz + czo + 2H_2O + Ca^{2+}	-62.207	-0.00905	5960.70	-4.137E-06	23.623	
$Ca^{2+}/(Na^+)^2$	4.5qtz + czo + 2Na^+ = 0.5pre + 2alb + Ca^{2+}	-148.541	-0.07365	5077.30	2.659E-05	62.247	
$Al(OH)_4^-$ H^+	czo + 3H_2O = pre + $Al(OH)_4^-$ + H^+	764.825	0.40530	-19383.80	-1.926E-04	-330.608	
$Fe(OH)_4^-$ H^+	epi + 3H_2O = pre + $Fe(OH)_4^-$ + H	-7.993	-0.00190	-3457.80	9.800E-07	-0.198	
Mg^{2+}/Ca^{2+}	chl+3wai+5Ca^{2+} = 4pre+3qtz+6H_2O+5Mg^{2+}	-458.604	-0.15774	8501.20	6.081E-05	181.398	

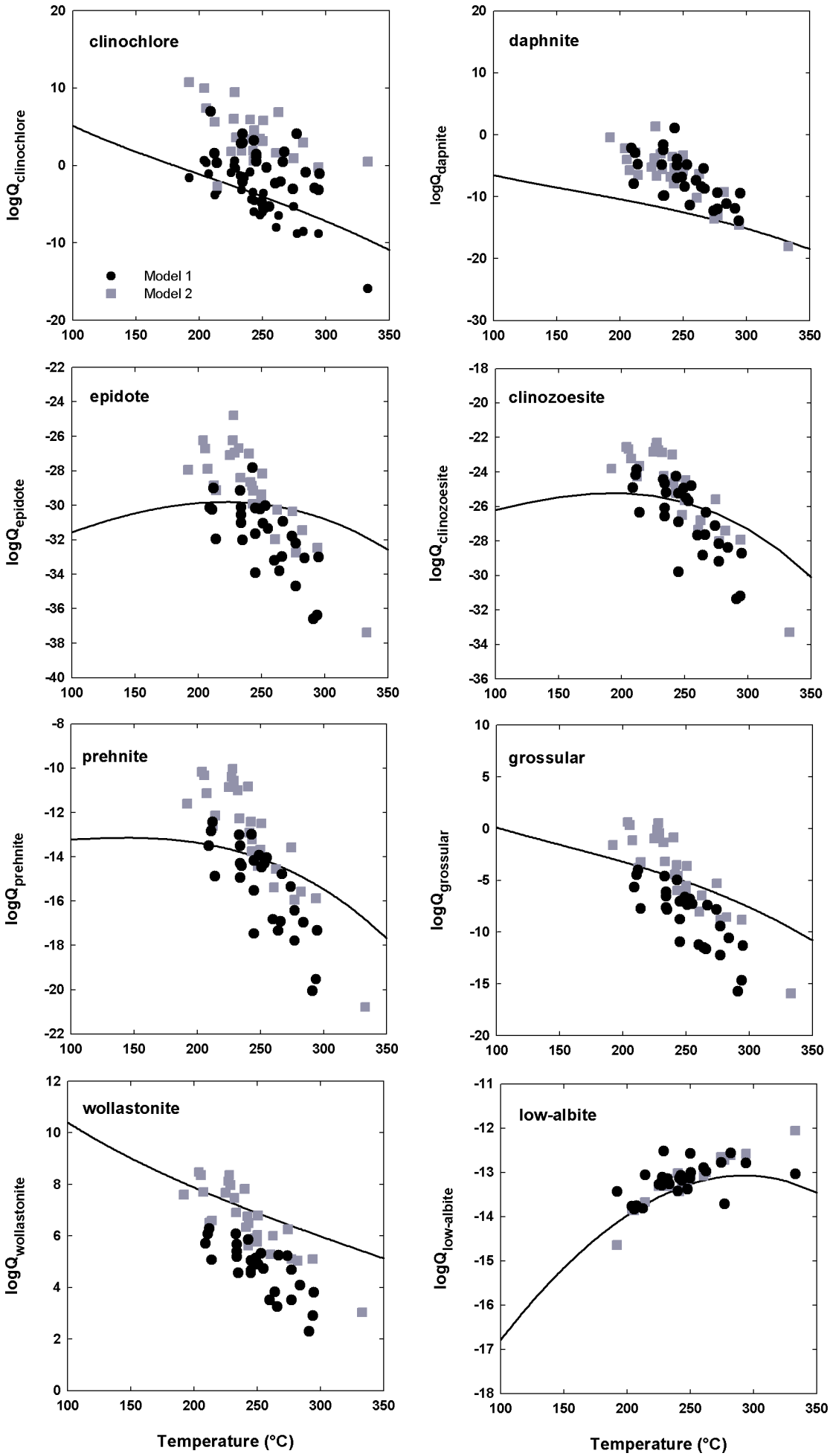

Figure 2.3a. Secondary mineral saturation state. The symbols show the reaction quotient calculated using models 1 and 2 (see text) and the lines show the equilibrium solubility of the respective minerals (Table 2.5).

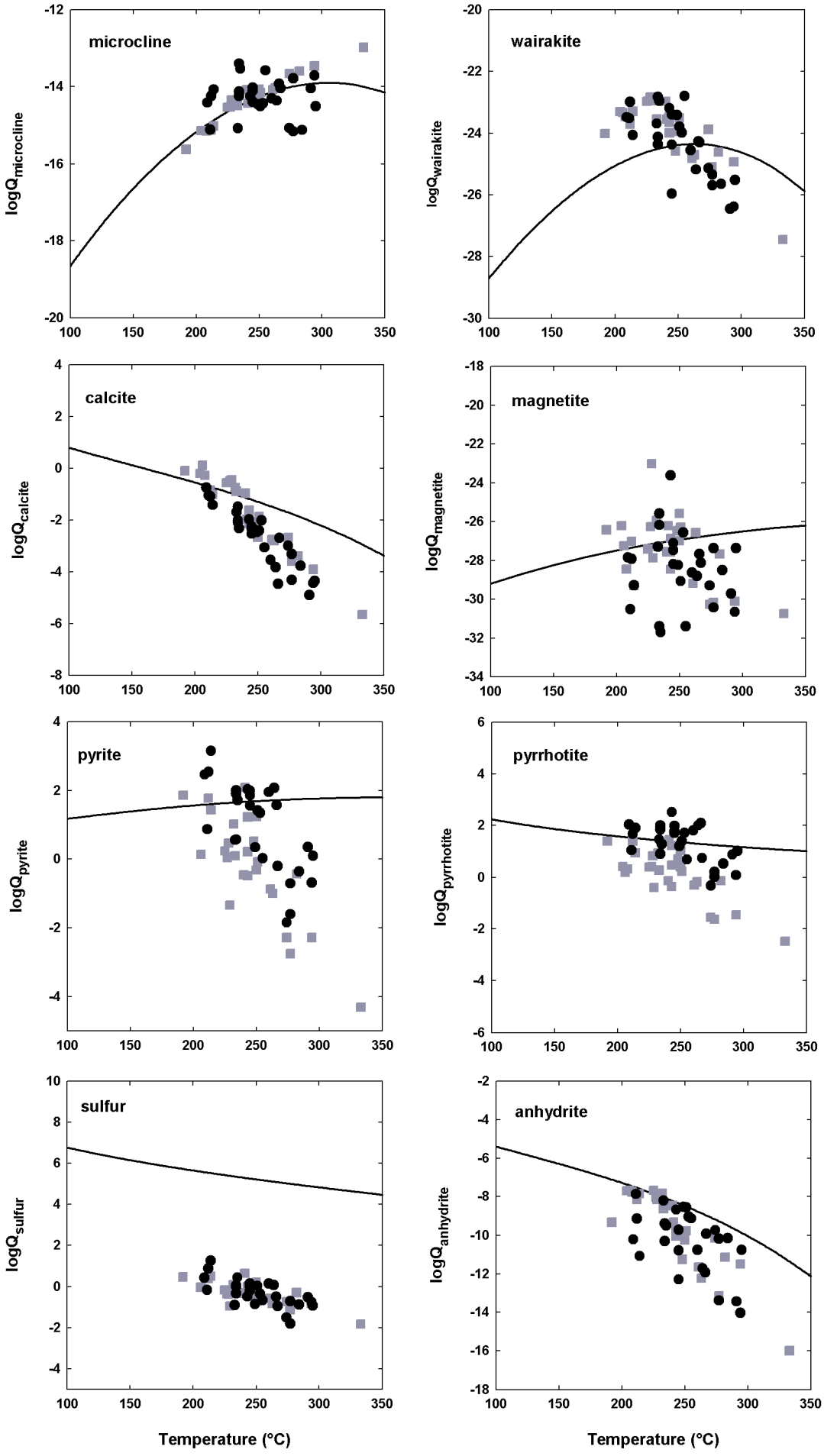

Figure 2.3b. Secondary mineral saturation state. The symbols show the reaction quotient calculated using models 1 and 2 (see text) and the lines show the equilibrium solubility of the respective minerals (Table 2.5).

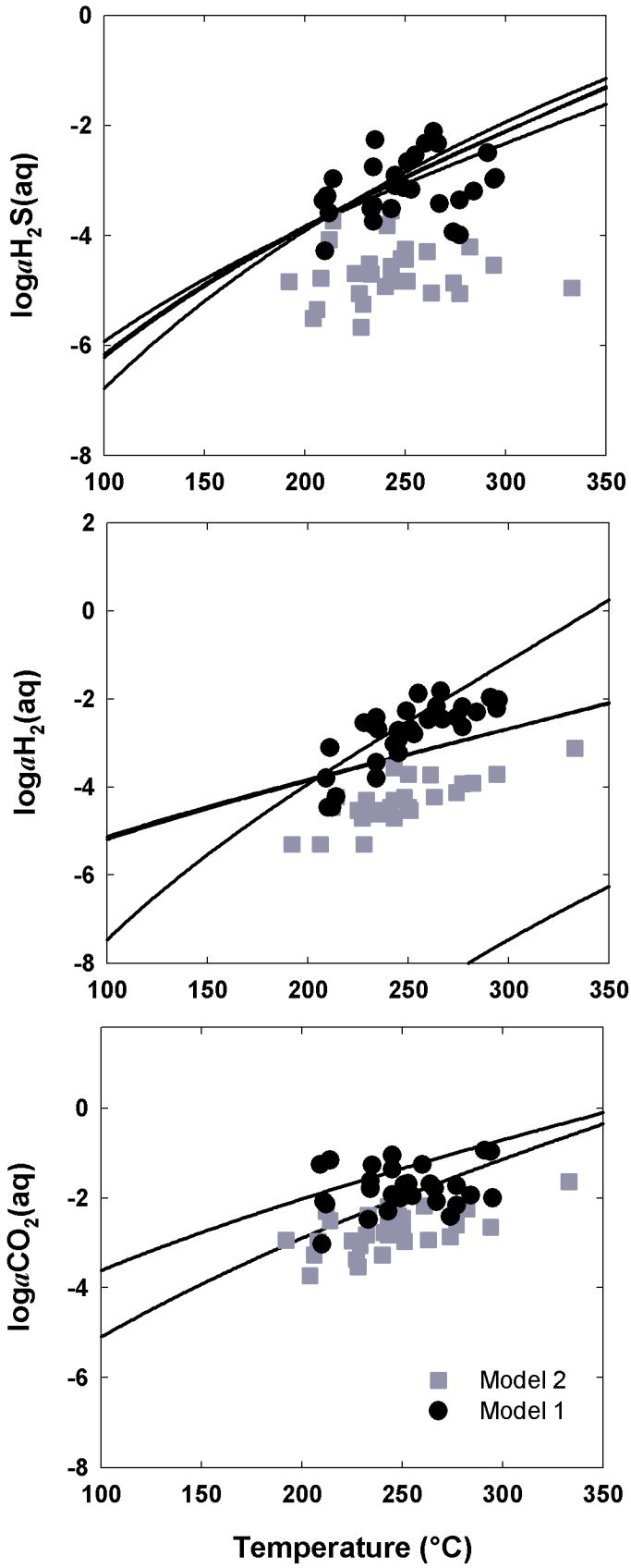

Figure 2.4. Equilibrium condition of CO_2, H_2S and H_2 in aquifer fluids in Krafla. The symbols show the gas concentration calculated using models 1 and 2 (see text) and the lines show the equilibrium solubility of various mineral buffer reactions (Table 2.6).

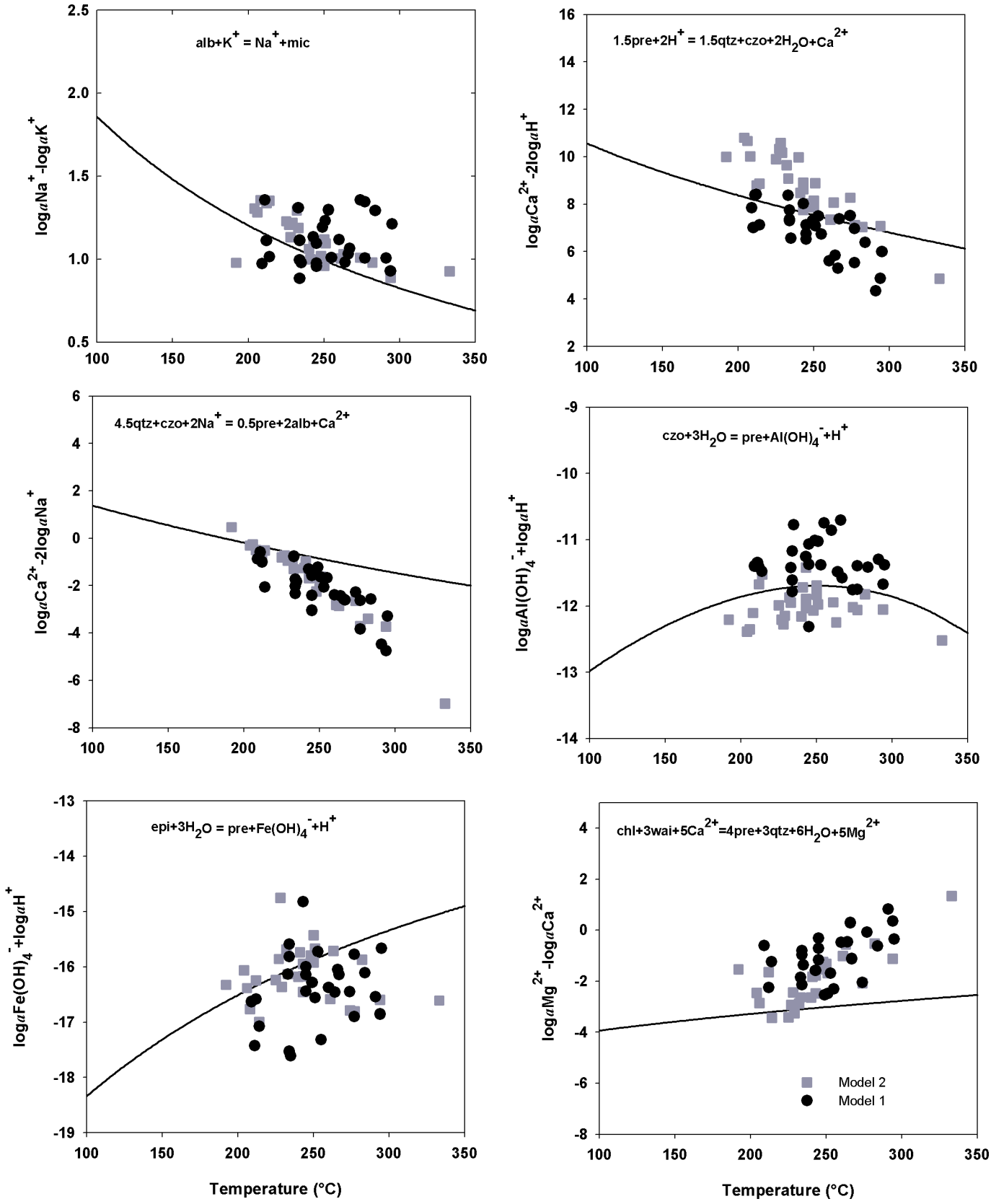

Figure 2.5. Equilibrium condition with respect to some plausible mineral buffer reactions. The symbols show the reaction quotient calculated using models 1 and 2 (see text) and the lines show the equilibrium solubility of the respective minerals (Table 2.6).

The results of the mineral saturation state calculations are shown in Figure 2.3. The results indicate that aquifer fluids are controlled close to equilibrium of the commonly observed secondary minerals in the Krafla system. Considerable scatter is observed in most cases as well as differences between model 1 and model 2 used for calculation of the reservoir fluid composition. The causes are considered to be various and include the calculation of reservoir fluid composition from data on well fluids collected at surface, thermodynamic data used for aqueous speciation including the calculation of reservoir fluid pH, and uncertainties of mineral solubility constants.

Based on these observations, mineral buffer reactions likely to control fluid chemistry in Krafla were constructed. The controlling reactions for various aqueous species and species ratios are given in Table 2.6 and the equilibrium mineral buffer reactions are compared with the actual conditions found for the reservoir fluids in Krafla in Figures 2.4 and 2.5. As observed, the concentrations of CO_2, H_2S and H_2 are all close to equilibrium with plausible mineral buffers; however, several buffers are possible that give similar concentrations and it is impossible to distinguish between them. Regarding the major elements, the various ion-ion rations closely approach equilibrium with plausible mineral buffer reactions.

These findings suggest that the chemical composition of geothermal fluids in the Krafla geothermal system is controlled close to equilibrium with common secondary minerals found in the system, the equilibrium condition depending on temperature. This is in line with previous results (e.g. Arnórsson et al., 1983; Stefánsson and Arnórsson, 2000, 2002; Gudmundsson and Arnórsson, 2005).

3 The chemistry of superheated vapor of IDDP-1

3.1 Sampling and analysis of single phase vapor fluids – IDDP-1

Superheated vapor is a single phase fluid and the vapor phase represents the total well discharge. Therefore, no separation of phases, like liquid and vapor, is necessary when sampling such fluids.

Water (H_2O) dominated superheated vapor cools down and expands readily upon depressurization. To prevent possible chemical changes upon sampling it is therefore important to prevent cooling as much as possible until the sample condenses into the sampling bottles used. This may be done by insulating all exposed valves and tubes used for sampling. Moreover, the sampling line needs to be as short as possible and be made of material that does not interact with the fluids. Metal parts should be avoided as much as possible and if needed, acid resistant metal should be used, for example titanium. Preferably, the sampling line can be made of silicon tubes and Pyrex glass (or silica glass), if possible.

Four samples were collected for major elemental analyses: pH, Si, B, Na, K, Ca, Mg, Fe, Al, F, Cl, CO_2, H_2, N_2, Ar, O_2, CH_4, S_{TOT}, H_2S, SO_4 and SO_2 concentrations.

The sampling layout is shown in Figure 3.1 and analytical methods are summarized in Table 3.1. The samples were collected into 125 ml gas bulbs, and using glass vapor condensers. Both were made of Pyrex glass. The sampling bulbs were connected directly to the outlet of the sampling well valve using a silicon tube. To prevent overpressure during sampling, a tee-piece either made of metal or Pyrex glass was placed in line with the silica tube, one outlet going to the sampling container and the other connected to a check valve. During sampling, outflow form the check valve should be observed at all times, to ensure a slight overpressure in the sampling line and minimizing the possibility of leakage and air contamination.

The various sample containers and protocols were designed in order to preserve the elements to be analyzed, both during sampling and upon storage.

Sample #1 was used for CO_2, H_2, N_2, Ar, O_2, CH_4 and S_{TOT} determination in the total discharge. The sample was collected into a Pyrex gas bulb containing ~30 ml 4 M NaOH. The base to sample volume did not exceed much over 1:1. In this way, the sample is diluted upon sampling, preventing possible metal precipitation and the alkaline pH value prevents elemental sulfur precipitation upon H_2S disproportionation/oxidation. The elemental concentrations were analyzed using titrations and GC.

Samples #2 and #3 were used for pH, Si, B, Na, K, Ca, Mg, Fe, Al, F and Cl analyses. The samples were collected into a Pyrex vapor condenser. A small volume of vapor condensates was collected (~10 ml) and then filtered into high-density polyethylene bottles

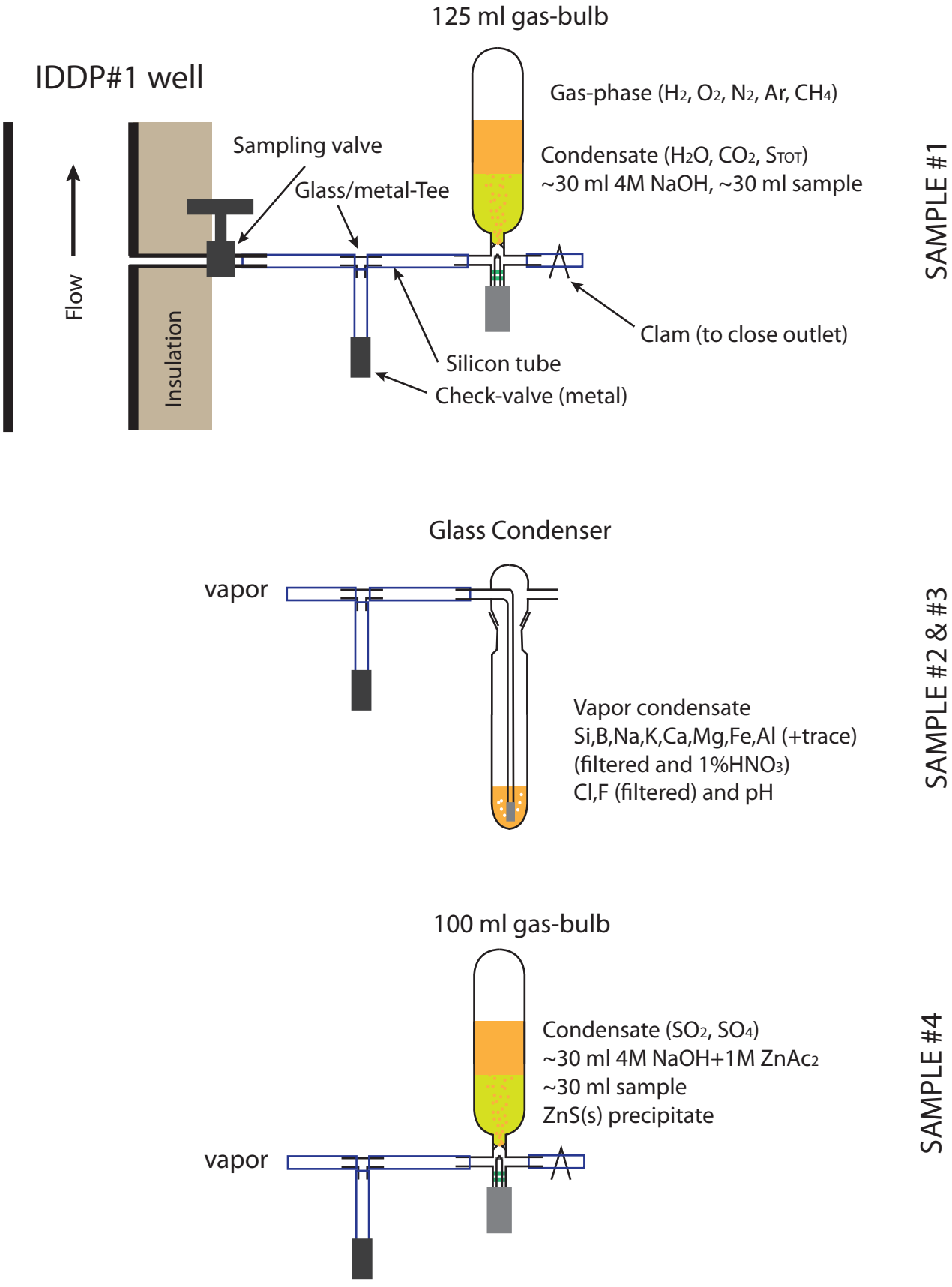

Figure 3.1. A schematic picture of the layout used for sampling superheated vapor from the IDDP-1 well.

Table 3.1
Summary of sampling treatment and analytical methods used for superhaetd vapor phase samples

Comonent	Sampling method	Analytical method	Standard and control samples [a]
pH	cooled, untreated, on-site	pH electrode	com. pH buffers
Si	condensed, filtered (0.2µm), 0.5% HNO_3	ICP-OES	spói05
B	condensed, filtered (0.2µm), 0.5% HNO_3	ICP-OES	spói05
Na	condensed, filtered (0.2µm), 0.5% HNO_3	ICP-OES	spói05
K	condensed, filtered (0.2µm), 0.5% HNO_3	ICP-OES	spói05
Ca	condensed, filtered (0.2µm), 0.5% HNO_3	ICP-OES	spói05
Mg	condensed, filtered (0.2µm), 0.5% HNO_3	ICP-OES	spói05
Fe	condensed, filtered (0.2µm), 0.5% HNO_3	ICP-OES	spói05
Al	condensed, filtered (0.2µm), 0.5% HNO_3	ICP-OES	spói05
Cl	condensed, filtered (0.2µm), 0.5% HNO_3	IC	com. standards
SO_4	condensed, filtered (0.2µm), 0.5% HNO_3	IC	com. standards
F	condensed, filtered (0.2µm), 0.5% HNO_3	IC	com. standards
CO_2	Gas bulb with 4M NaOH	Titration	prim. meas.
H_2S	Gas bulb wit 4M NaOH	IC	com. standards
SO_2	Gas bulb wit 4M NaOH, 1M $ZnAc_2$	IC	com. standards
H_2	Gas bulb wit 4M NaOH	GC	air and com. standards
CH_4	Gas bulb wit 4M NaOH	GC	air and com. standards
N_2	Gas bulb wit 4M NaOH	GC	air and com. standards
Ar	Gas bulb wit 4M NaOH	GC	air and com. standards
O_2	Gas bulb wit 4M NaOH	GC	air and com. standards

[a] prim. measurements = primary standard measurements, i.e. no standard needed; spói95 = University of Iceland in-house ICP-OES standard used for geothermal waters, based on comercial certified standards; com. standards = comercial certified standards.

(HDPE) using a 0.2 µm cellulose acetate filter. Sample #2 for major cation determination (Si, B, Na, K, Ca, Mg, Fe and Al) was acidified to 0.5% HNO_3 (Suprapur® Merck) and analyzed using ICP-AES, and the sample for anion determination was not further treated but analyzed using IC as well as being used for on-site pH determination using a pH electrode.

Sample #4 was used for sulfur species determination including H_2S, SO_4 and SO_2 concentrations. The sample was collected into a Pyrex gas bulb containing ~20 ml 4 M NaOH and ~10 ml 1M Zn-acetate and the NaOH+Zn-acetate solution to sample volume did not exceed much over 1:1. The H_2S in the vapor adsorbs into the base and is immediately precipitated, forming solid zink sulfide (ZnS(s)). The bottle is then opened and the ZnS(s) precipitate filtered off, and the filtered solution collected into a polypropylene bottle. One filtered aliquot of the filtered solution was analyzed on-site for SO_4, whereas another aliquot was oxidized and analyzed for the sum of SO_4 and SO_2. Combined with the total sulfur concentration in the vapor condensate (S_{TOT}) the various sulfur species concentrations may be calculated. All analyses were carried out using ion chromatography.

Pre-flushing of sample line and sample well valve was observed to be very important in order to get reproducible results. The sampling setup should be pre-flushing for at least

Table 3.2

Chemical composition of vapor from IDDP#1collected at the well-head

Element	12-KRA-01	12-KRA-02	12-KRA-03
pH/°C [a]	2.65/17	2.58/19	2.25/21
SiO_2	8.25	3.79	5.69
B	1.07	1.61	1.52
Na	0.44	0.24	0.81
K	0.20	0.11	0.06
Ca	0.34	0.10	0.09
Mg	0.05	0.02	0.01
Fe	2.29	10.81	2.59
Al	0.10	0.06	0.03
As	0.05	0.06	0.05
Mn	0.04	0.22	0.04
CO_2	2108.00	1310.00	1500.00
S_{TOT}	642.00	589.00	583.00
SO_2	nd	nd	nd
H_2S	620.92	575.52	569.55
SO_4	21.08	13.48	13.45
F	11.21	14.65	13.34
Cl	79.60	117.60	118.40
Br	0.22	0.38	0.43
H_2	19.53	15.26	15.27
N_2	196.00	866.00	780.00
Ar	4.81	17.88	16.57
CH_4	0.58	0.89	0.64

[a] pH of the vapor condensate - should not be taken as the pH of the superheated vapor

as long as possible (at least 10-20 minutes) at as high a flow rate as before sampling. Failure to do this was observed to result in enrichments of various elements, for example Si and Fe, and considerable aerosols/particles in the fluid discharge.

3.2 The chemical composition of the IDDP-1 vapor

The chemical composition of IDDP-1 vapor is given in Table 3.2. The chemical compositions used in this report are based on samples collected and analyzed by scientists at the University of Iceland and discussed above (section 3.1).

The chemical composition of the IDDP-1 vapor is characterized by elevated concentrations of volatiles and depleted concentrations of non-volatiles compared to single phase liquid and two-phase liquid and vapor fluids in Krafla. The volatiles included CO_2, H_2S as well as Cl, F and B. The non-volatiles included Na, K, Ca, Mg, Al, Fe and SO_4, their concentrations being <1 ppm in all cases. Silica differs as it was found in considerable high

concentration in the IDDP-1 vapor compared to other non-volatiles, yet it was observed in low concentrations compared to geothermal water, i.e. ~10-20 ppm in the IDDP-1 vapor compared to 400-600 ppm in geothermal waters.

The results of the chemical composition of the IDDP-1 vapor were found to be very dependent on sampling method. The pH of the vapor condensation was observed to be low, pH <3. Such vapor condensation is corrosive and may dissolve the material of the sampling containers, particularly metal parts. Therefore, it is important only to use glass (silica or Pyrex) and silicon tubes when sampling superheated steam.

3.3 Formation of superheated vapor in the Krafla system

The vapor discharging the IDDP-1 well had a temperature of ~450°C and pressures of ~140 bar (Markússon et al., 2013). Other wells in Krafla have shown possible indications of superheated vapor in terms of high gas content and low pH of the fluids. The wells include KG-4, KJ-7, KG-10, KG-25, KG-26, KJ-27, KJ-29, KJ-33, KJ-35, KJ-36, KJ-38 and KJ-39 (e.g. Hauksson, 2008; Einarsson et al., 2010). The possible source of such superheated vapor may be related to input of volcanic gas into the geothermal system by magma degassing and/or excessive heat transfer to single liquid phase or two-phase geothermal fluids (Hayba and Ingenbritsen, 1997; Driesner and Geiger, 2007). It may be difficult to distinguish between the two types as the ultimate source of many volatiles in geothermal and volcanic fluids is magma, either through degassing or upon dissolution by fluids of solidified magma.

Based on the findings of Hayba and Ingenbritsen (1997) it is probable that the source of the superheated vapor discharging IDDP-1 is geothermal water within that has flowed close to a fresh (young) intrusion (pluton) at relatively shallow depth (ca. 2 km depth). The superheated vapor forms upon addition of heat, for the hot intrusion, to the geothermal water. Upon such addition of energy (enthalpy) to the geothermal water at a pressure below the critical pressure of water, the geothermal water starts to boil and may boil to dryness or single phase superheated vapor (Fig. 3.2). Assuming closed system boiling, the physiochemical system will maintain close to constant temperature at constant pressure during the boiling process. The addition of heat will simply lead to progressively increased vapor fraction (X^{vapor}) within the fluid system. When the water has boiled to dryness and the system consists of a single vapor phase, the temperature may rise again. The pressure may also increase, depending on the depth-related flow path of the fluids (Fig 3.2). The process of heat addition by intrusion is shown schematically in Figure 3.2 based on models of Hayba and Ingenbritsen (1997). According to the models, such superheated vapor formation is characteristic of early stages of geothermal systems intruded by a hot magma; however, with continuous cooling of the intrusion the fluid phase relations change to two-phase systems and eventually to sub-boiling systems. The fraction of vapor at depth may be as high as 100%, i.e. single phase superheated vapor. Alternatively, the temperature, pressure and

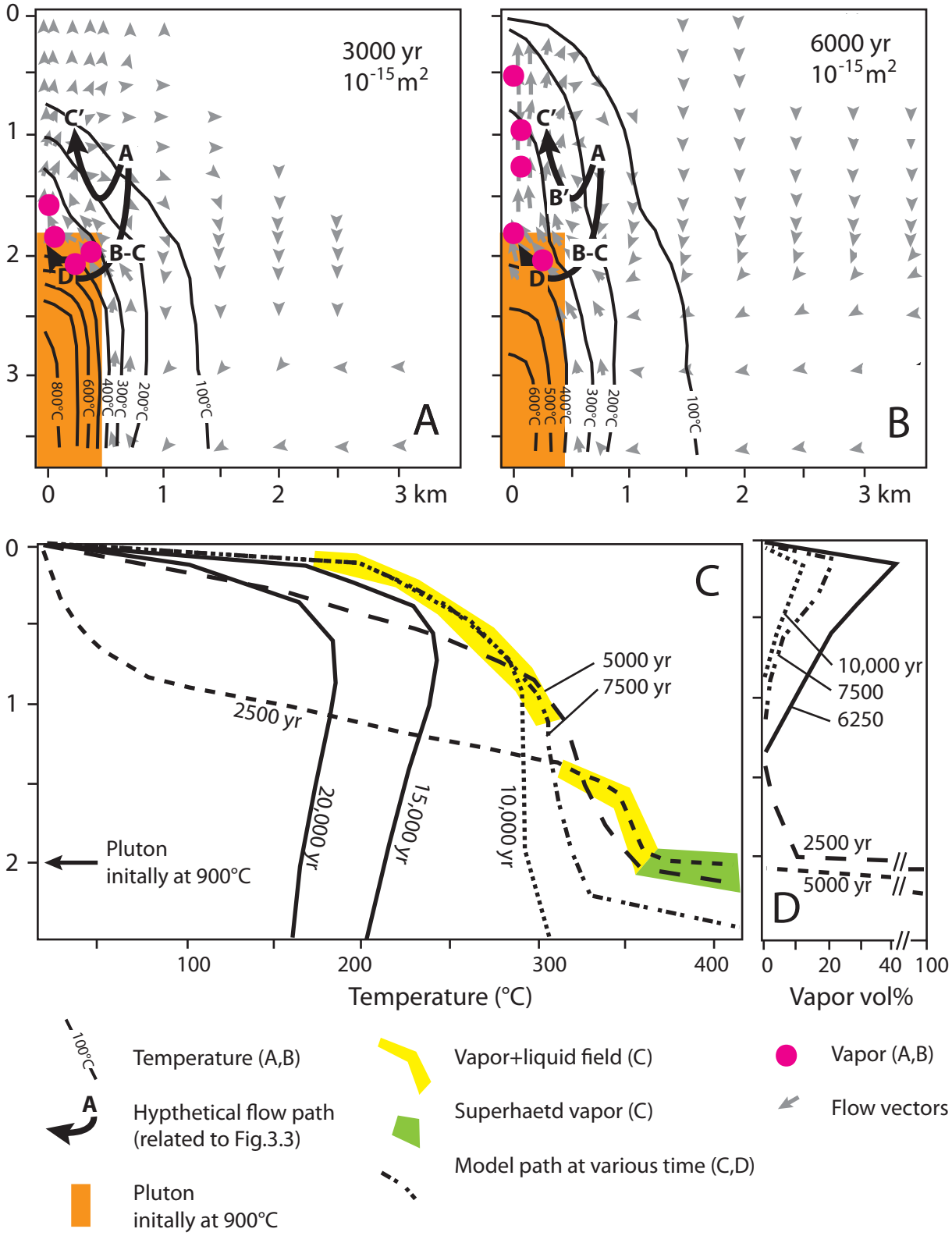

Figure 3.2. A conceptual model of a hypothetical geothermal system as a function of time having a pluton at 2 km depth and initial temperature of 900°C and host rock permeability of 10-15 m2. Note at temperatures greater than 260°C, permeability decreased with increasing temperature. (A) and (B) show flow vectors and temperature contours after 3000 and 6000 yrs. of geothermal system developments. Also shown are possible fluid flow paths (A-B-C-D) that can lead to production of two-phase geothermal fluids (liquid and vapor) and single phase superheated vapor. The paths shown are referred to the paths in Figure 3.3. (C) Temperature-depth profiles above the center of the pluton (along the left side of models shown in A and B) at selected times and (D) profiles showing volumetric properties of vapor at the same location and time. The pictures are based on results of Hayba and Ingebritsen (1997).

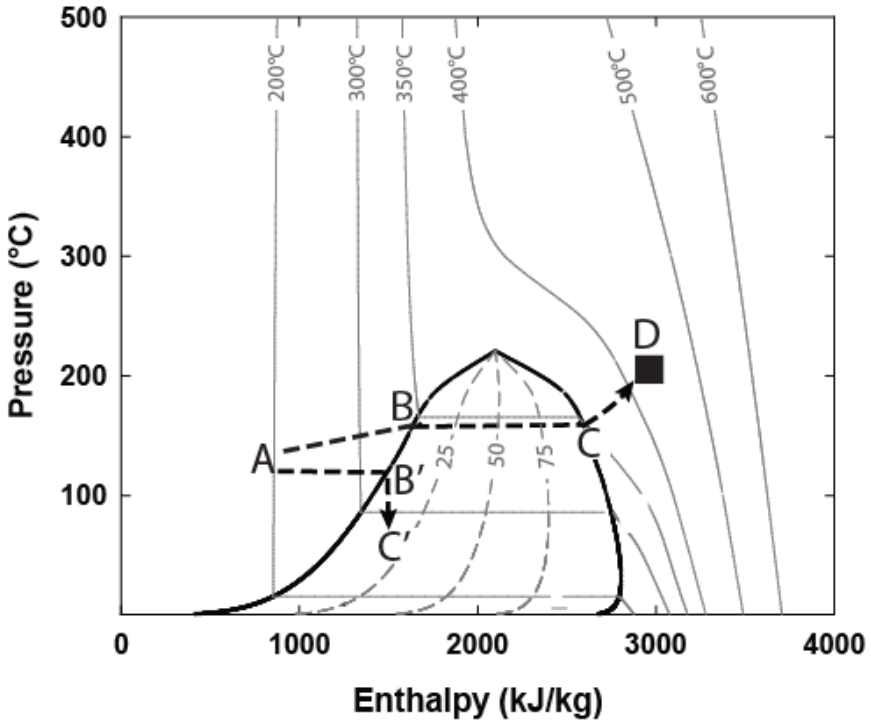

Figure 3.3. *The phase relationship associated with the possible formation of superheated vapor in Krafla through energy (enthalpy) addition to geothermal water. At (A) single phase liquid only geothermal water exists in the system at temperatures of ~270°C. Upon head input measured by increased enthalpy (h) the water starts to boil (path A to B), the ratio of vapor to water increasing with increasing enthalpy. Under these conditions, the temperature is fixed at fixed pressure or depth. When the two-phase fluids reach vapor saturation (~2700 kJ/kg) (B) all the water has been boiled to vapor and the fluid moves into the field of superheated vapor, where temperature starts to increase with increasing enthalpy. Pressure may also change depending on the hydrological movement of the vapor. Hypothetically, the fluid eventually reaches the state of IDDP-1 at depth taken to be ~450-500°C and 150-200 bar.*

enthalpy relation of the physiochemical system of such a young to moderately young geothermal system are further shown in Figure 3.3. The exact pressure temperature relations do not exactly match with those shown in Figure 3.2 as these depend not only on the properties of water (as for Fig. 3.3) but also on hydrology and heat transfer (as for Fig. 3.2), but schematically they mimic each other in terms of the A-B-C-D paths shown in the figures.

The chemical consequences of such boiling of geothermal water to dryness and formation of superheated vapor were simulated using conservation of mass and energy. The calculations were carried out using the WATCH program (Arnórsson et al., 1982; Bjarnason, 2010) in combination with the PHREEQC program (Parkhurst and Appelo, 1999) well as the HSc chemistry (http://www.outotec.com) for the vapor phase.

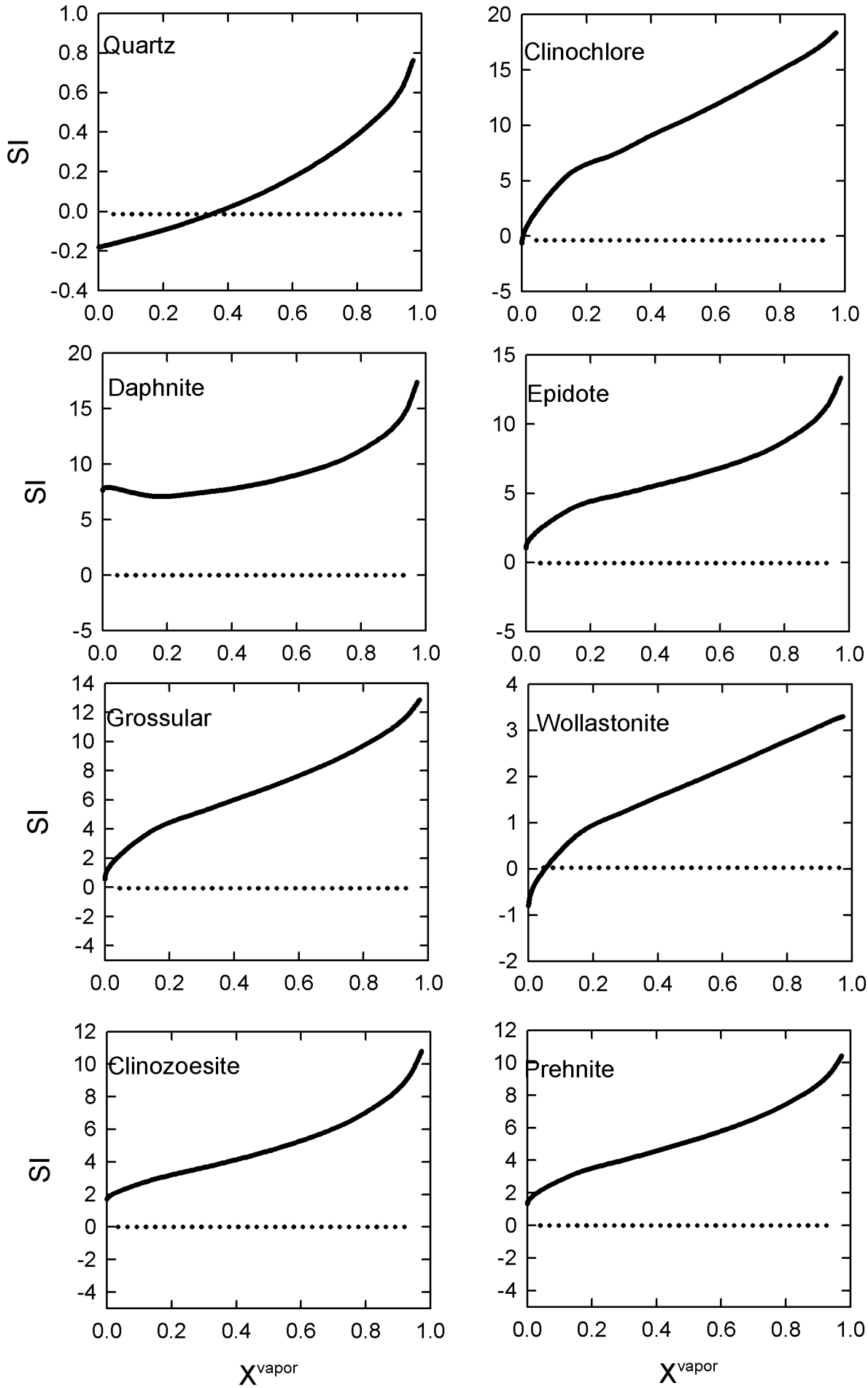
Quartz
Clinochlore
Daphnite
Epidote
Grossular
Wollastonite
Clinozoesite
Prehnite
SI
SI
SI
SI
X^vapor
X^vapor

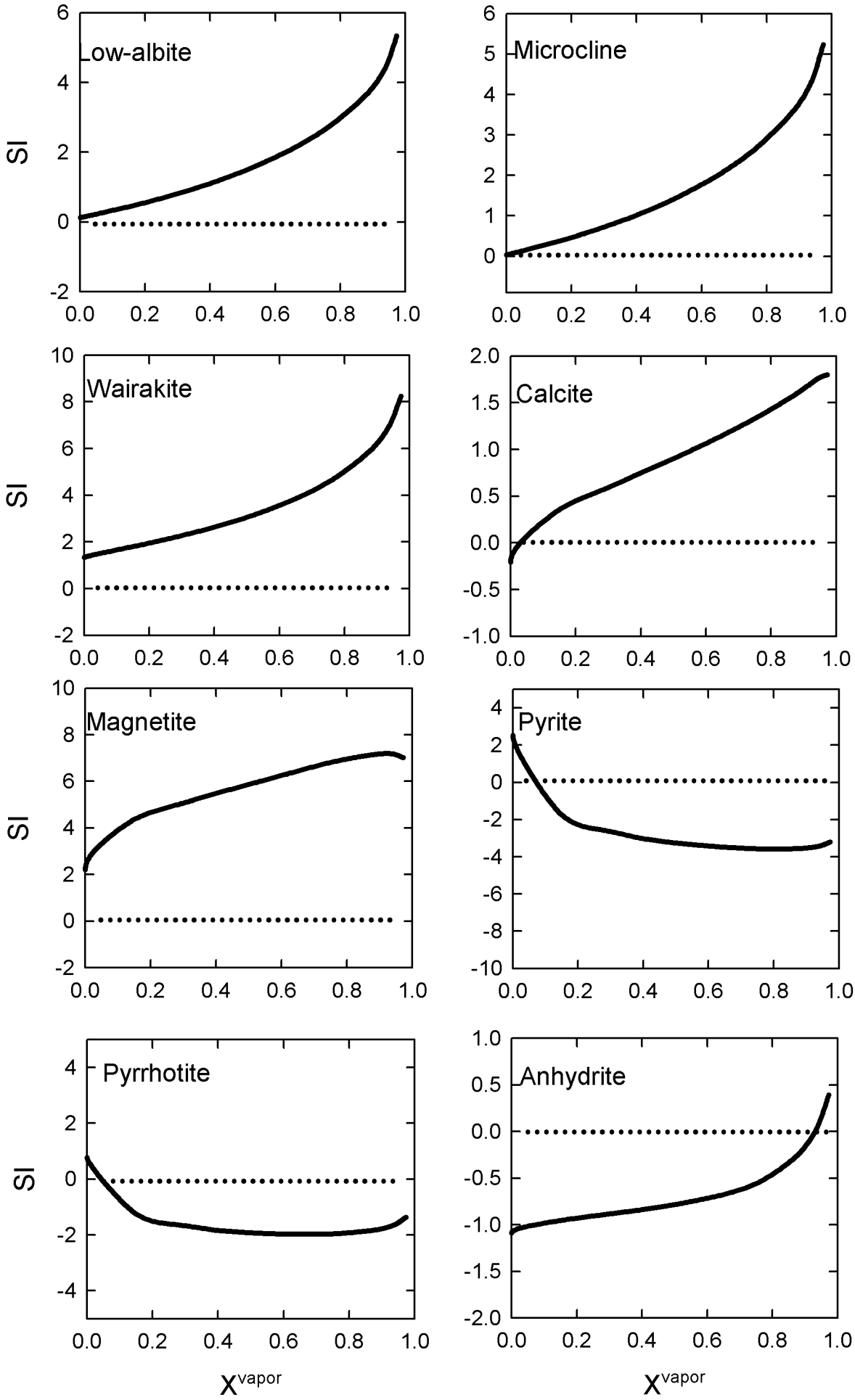
Low-albite
Microcline
Wairakite
Calcite
Magnetite
Pyrite
Pyrrhotite
Anhydrite
SI
SI
SI
SI
X^vapor
X^vapor

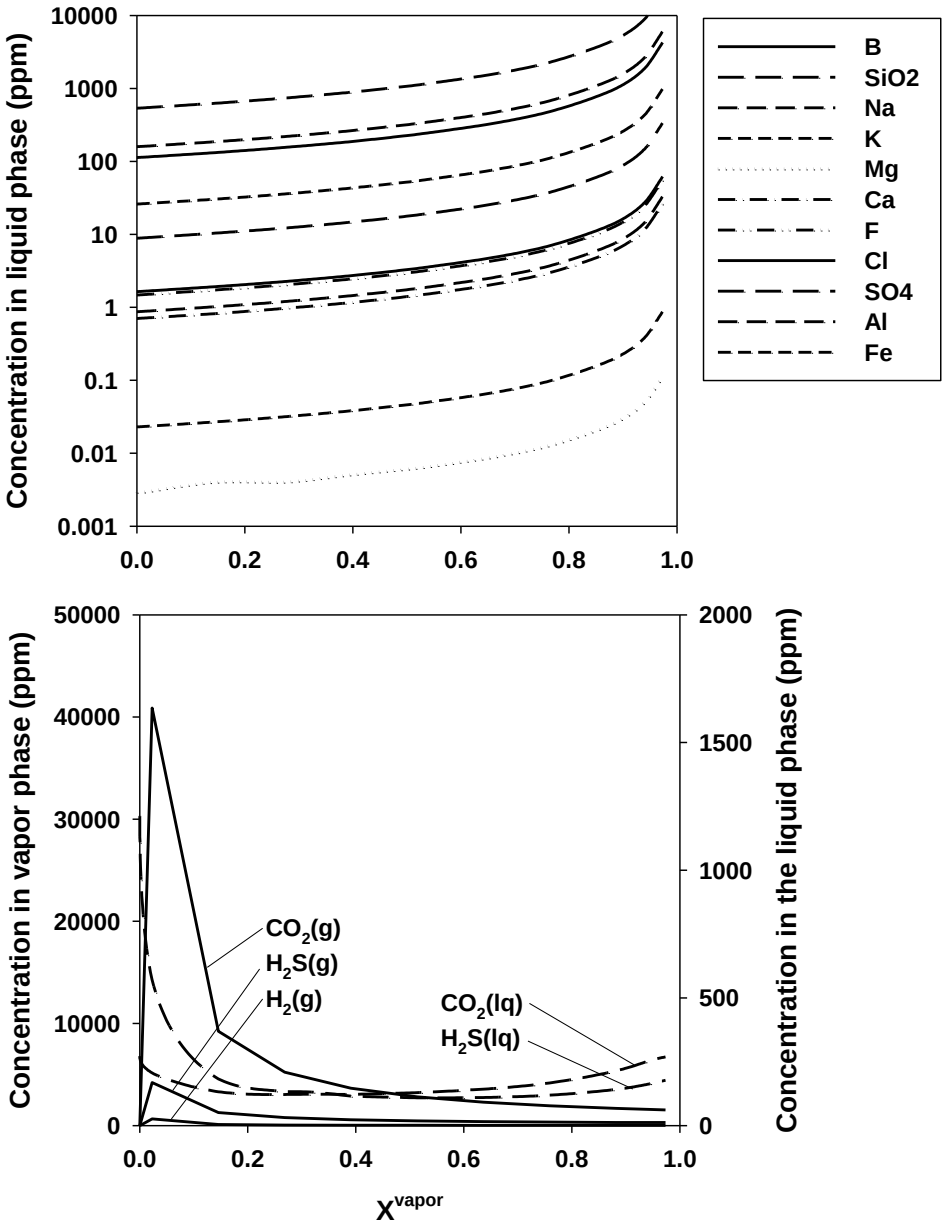

Figure 3.4. *The concentration of elements in the liquid and vapor phase upon boiling of geothermal water at 265°C (Table 3.3) at constant pressure and temperature but increased enthalpy. The path corresponds to B-C in Figures 3.2 and 3.3. The concentration of the non-volatiles increases in the liquid phase upon boiling due to loss of water to the vapor phase, whereas the volatile components quantitatively enter the vapor phase upon boiling, their concentration being high in the initial vapor bubble but decreasing as the mass of vapor increases upon continuous boiling.*

Two types of models were carried out. In the first approach, the composition of water and vapor upon boiling at constant temperature and pressure but variable enthalpy was calculated. From the results, the aqueous speciation and mineral saturation indices were calculated. In the second approach, the composition of water and vapor upon boiling at constant temperature and pressure but variable enthalpy was calculated and allowing supersaturated secondary minerals to precipitate upon boiling. The minerals included the

Figure 3.5. *(previous two pages) The mineral saturation indices (SI) for common geothermal minerals upon boiling Krafla geothermal water from pure liquid water ($X^{vapor} = 0$) to pure vapor ($X^{vapor} = 1.0$). SI <0 indicates undersaturation, SI = 0 indicates equilibrium saturation and SI>o indicates supersaturation and potential mineral formation. As indicated, almost all secondary minerals have the potential to form upon boiling at constant temperature and pressure and increased enthalpy, resulting in a decrease of the mineral forming elements in the liquid boiled water phase.*

common geothermal minerals: quartz or amorphous silica, anhydrite, calcite, clinochlore, clinozoesite, daphnite, epidote, grossularite, low albite, magnetite, microcline, prehnite, pyrite, pyrrhotite, sulfur, wairakite and wollastonite. Their solubility was taken from Table 2.5. The composition of the starting water used in the calculations is given in Table 3.3 and represent typical geothermal aquifer water in Krafla at a temperature >250°C.

The results of the former approach are shown in Figures 3.4 and 3.5. As observed, the boiling led to increased concentration of non-volatiles in the boiled liquid water. This increased concentration of Si, Al, Fe, Mg and Ca led to supersaturation of common secondary minerals. The volatiles including H_2S, CO_2 and H_2 quantitatively entered the vapor phase upon initial boiling, their concentration being very high in the first vapor formed and then decreasing with enhanced boiling and mass vapor formation.

The results of the second approach were secondary minerals allowed to form upon boiling when supersatured, as shown in Figure 3.6. The concentrations of non-volatiles including Al, Fe, Ca and Mg almost instantaneously decreased to very low concentration in the boiled system due to mineral formation. Silica precipitation was also significant as the fluids were boiled to dryness; however, the exact concentration depended on whether quartz or amorphous solubility was chosen. Regarding Na and K, these elements enter secondary feldspars (albite and microcline); however, their formation was limited by the very low availability of Al in the system due to formation of other secondary minerals, and hence only an insignificant formation of feldspar was observed upon boiling, resulting in a limited loss of Na and K. Whether this is truly the case is not certain at this point, but it needs to be kept in mind that the results of the calculations are very sensitive to the exact solubility of the secondary minerals. On the other hand, the volatile and mobile elements including H_2S, CO_2, H_2, Cl, F and B did not show any changes in total fluid composition upon boiling. The H_2S, CO_2 and H_2 entered the vapor phase, but such partitioning is not taken into account in the present day modelling for Cl, F and B.

Upon boiling of the geothermal water to single phase vapor (dry steam), the chemistry of the superheated vapor was simulated assuming equilibrium with common secondary minerals (quartz or amorphous silica, anhydrite, calcite, clinochlore, clinozoesite, daphnite, epidote, grossularite, low-albite, magnetite, microcline, prehnite, pyrite, pyrrhotite, sulfur, wairakite and wollastonite) using the HSc chemistry program (http://www.outotec.com) at a temperature of 450°C and pressure of 200 bars. The mobile

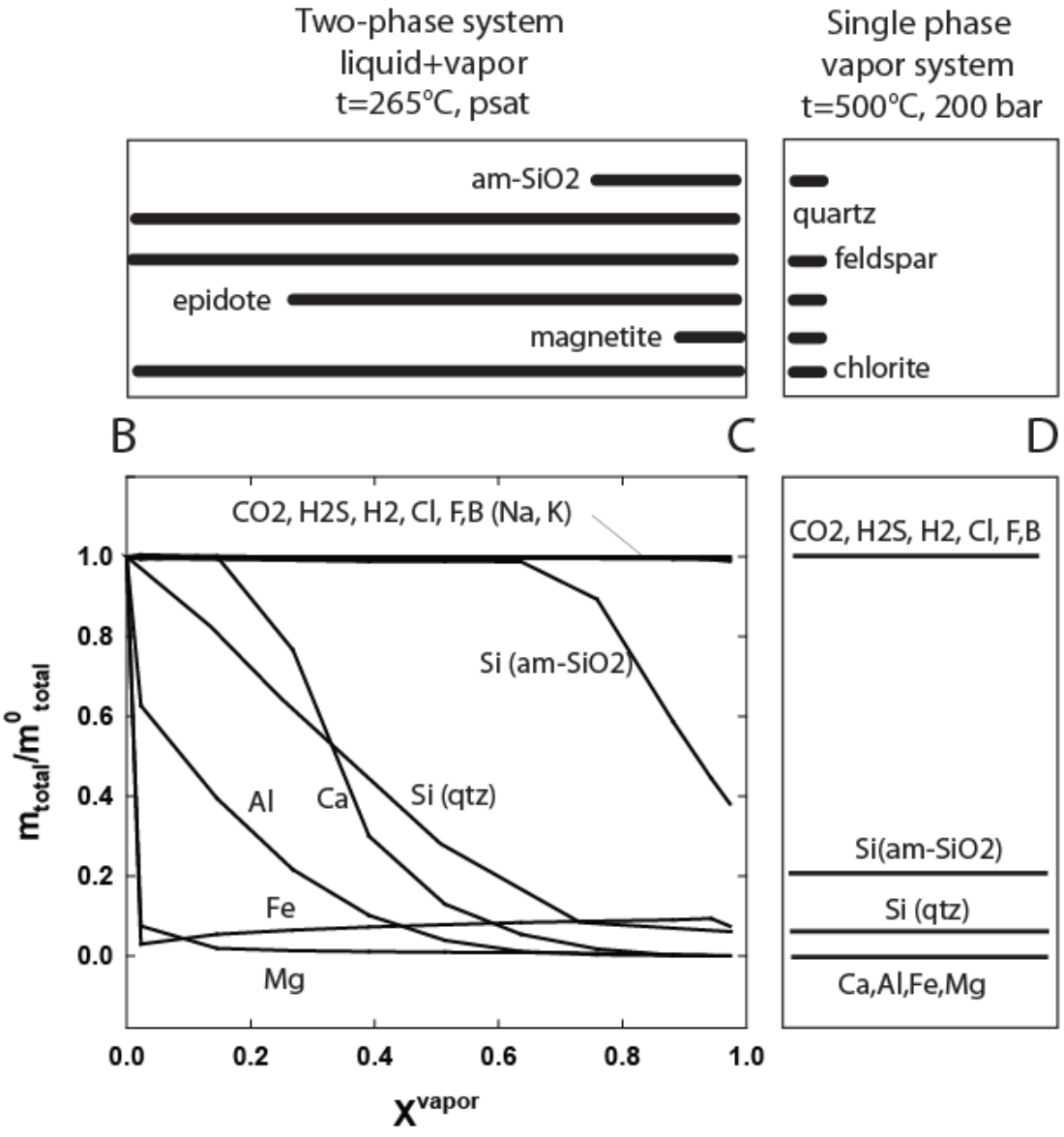

Figure 3.6. *Elemental transport upon boiling and vapor formation. Shown are the secondary mineral formation as a function of steam fraction (X^{vapor}) as well as the elemental mobility in the two-phase region and single phase region.*

elements Cl, F and B and the volatiles CO_2, H_2S and H_2 were observed to be stable and to enter the superheated vapor. The speciation for the volatiles was observed to stay the same upon boiling, CO_2(g), H_2S(g) and H_2(g), whereas the mobile elements were complexed or hydrolyzed to form HCl(g), HF(g) or SF_2Cl(g) and $B(OH)_3$(g) species in the superheated vapor (Table 3.3). The non-volatiles including Na, K, Ca, Mg, Fe and Al were, on the other hand, quantitatively removed from the vapor into secondary minerals resulting in concentrations of <1 ppm in superheated vapor. The silica concentration was found to be similar in the vapor phase at 450°C and 200 bar as in the last drop of water at 265°C, i.e. ~50-150 ppm SiO_2 depending on whether quartz or amorphous solubility was used to constrain the Si concentration.

Table 3.3

Fluid composition associated with modelling of the formation of superheated vapor in Krafla similar to the IDDP-1 vapor

Element	Unit	Krafla geothermal water [a]	Dominant species [b]	Modelled IDDP-1 vapor [c]	Dominant Species [d]	Measured IDDP-1 vapor
t	°C	265		450		450
p	bar			200		140
h	kJ/kg	1160		3200		
pH_T		6.60				
SiO_2	ppm	535	H_4SiO_4	50	H_2SiO_3	6
B	ppm	1.65	$B(OH)_3$	1.65	$B(OH)_3$	1.4
Na	ppm	160	Na^+	<1	Na_2Cl_2	0.5
K	ppm	25	K^+	<1	K_2Cl_2	0.12
Ca	ppm	1	Ca^{2+}	<1	$CaCl(OH)$, $CaCl_2$	0.18
Mg	ppm	0.003	Mg^{2+}	<1	$Mg(OH)_2$	0.03
Fe	ppm	0.02	Fe^{2+}, $Fe(OH)_4^-$	<1	$Fe(OH)_2$	2.4
Al	ppm	1	$Al(OH)_4^-$	<1	$Al(OH)_3$	0.07
CO_2	ppm	1500	HCO_3^-, CO_2	1500	CO2	1640
H_2S	ppm	300	HS^-	300	H_2S	590
SO_4	ppm	10	SO_4^{2-}			16
F	ppm	1.5	F^-	1.5	SF_2Cl	13.1
Cl	ppm	110	Cl^-	110	HCl	105
H_2	ppm	15	H_2	15	H_2	16.7

[a] The input water composition for the modelling of IDDP-1 vapor composition

[b] The Dominant aqueous species in the water phase according to PHREEQC and WATCEQ database (Parkhurst and Appelo, 1999)

[c] Modelled IDDP-1 vapor compostion at sampling conditions. The concentration of non-volatiles is listed as <1 ppm, the actual modelled values were neglable

[d] Dominant gas species in superheated vapor calculated using HSc chemistry. Note that there is no pH (activity of H+) given as H^+ does not calculate to be present in vapor.

The modelled chemical composition of superheated vapor formed on boiling of geothermal water by head addition is compared with the composition of the IDDP-1 fluids in Table 3.3. As seen, remarkably similar results were obtained with the exception of Si. Significantly lower values were observed in the IDDP-1 vapor than computed upon boiling of geothermal waters to superheated vapor. As discussed later, this may be related to the silica formation upon depressurization of superheated vapor occurring upon depressurization within the wellhead of IDDP-1 and during sampling. The fluid chemistry and scaling of silica is discussed in the next section.

3.4 Silica solubility in two-phase systems and in single phase vapor

Quartz (SiO_2) solubility has been measured over a wide range of temperature and pressure (e.g. Kennedy, 1950; Manning, 1994; Rimstidt, 1997). For the purpose of geothermal fluids ranging from single phase liquid to single phase vapor the formulation postulated by Fournier and Potter (1982) is very useful as they describe the solubility as a function of the specific volume of the fluid. The solubility of quartz according to the reaction

$$SiO_2(s) = SiO_2(fluid)$$

is given by the equation

$$\log m_{Si} = A + B \cdot \log V + C \cdot \log V^2$$

where m_{Si} is the molal concentration of silica in the fluid, V is the specific volume of water and the parameters A, B and C are given by

$$A = -4.66206 + 0.0034063 \cdot T + 2179.7 \cdot T^{-1} - 1.1292 \cdot 10^{-6} \cdot T^{-2} + 1.3543 \cdot 10^{8} \cdot T^{-3}$$

$$B = -0.0014180 \cdot T - 806.9 \cdot T^{-1}$$

$$C = 3.9465 \cdot 10^{-4} \cdot T$$

It should be noted that the form of silica in the fluid is written here as SiO_2(fluid). This is a thermodynamic convention. This does not necessarily indicate the true speciation of silica in the various phases; in fact according to the speciation calculations the dominant form of dissolved silica in water is H_4SiO_4(aq) and H_2SiO_3(g) in the vapor phase.

The solubility of quartz is shown in Figure 3.7. As shown, the solubility increases with increasing temperature or enthalpy for single phase liquid water. At ~300°C, the solubility starts to decrease into the supercritical and or superheated steam region. Quartz solubility is almost independent of pressure below 500 bars at low temperatures, but becomes important at temperatures above 300°C, increasing with increasing pressure and dramatically decreasing with decreasing pressure for superheated vapor. In the relation with the possible temperature and pressure path leading to the formation of superheated vapor of the IDDP-1, the solubility of silica decreases from the single phase liquid water phase to the single vapor phase region.

The solubility of silica has also been determined for two-phase systems, i.e. where vapor and water coexist. The solubility of silica in the vapor phase has been recently reviewed and is given by the formulation (Bahadori and Vuthaluru, 2010)

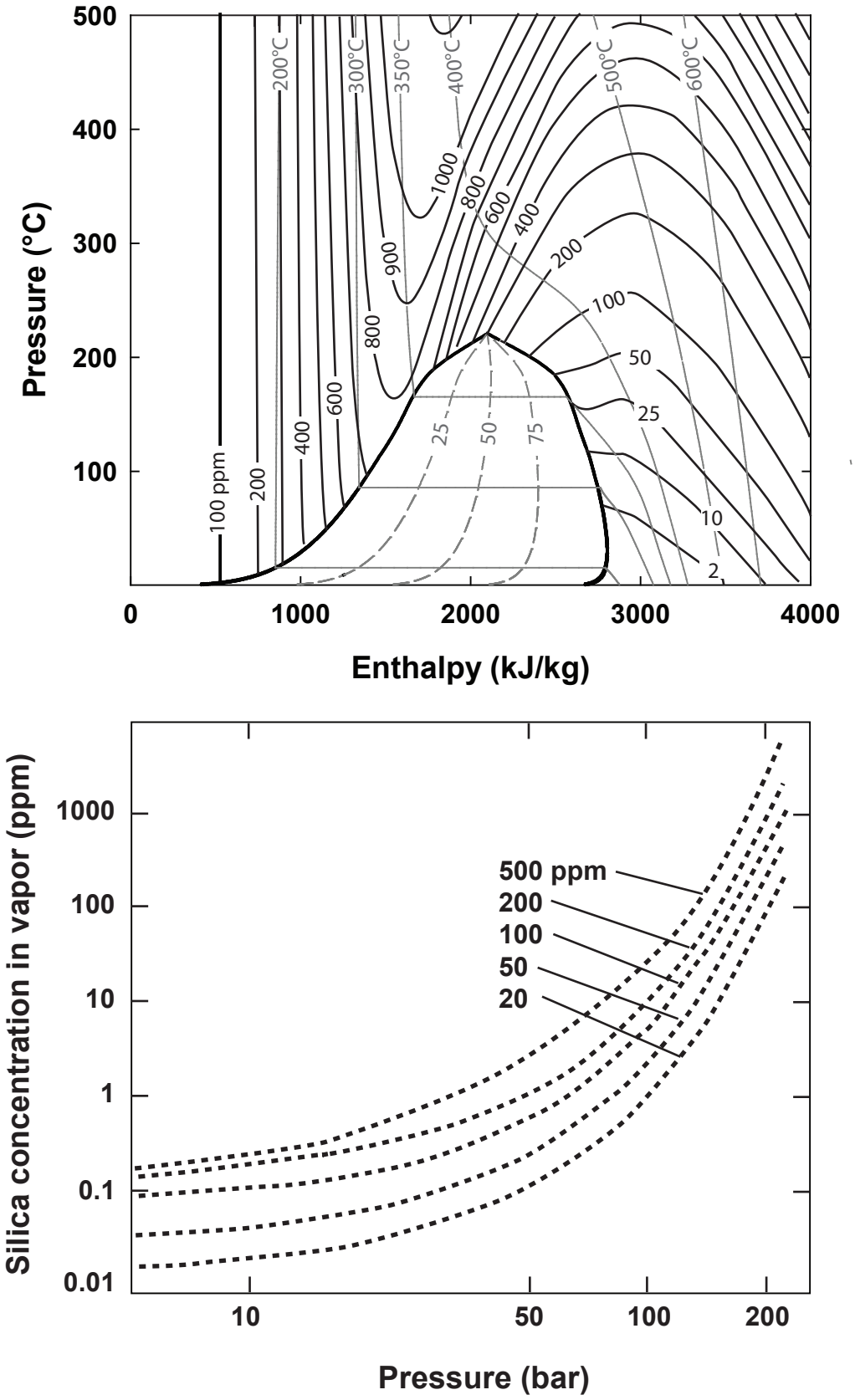

Figure 3.7. The solubility of quartz as a function of temperature and pressure and enthalpy and in the two phase lq+v region, calculated based on formulation given by Fournier and Potter (1982) and Bahadori and Vuthaluru (2010), respectively.

$$\ln m_{Si}^{v} = a + bp + cp^2 + dp^3$$

where m_{Si}^{w} is the silica concentration in the vapor phase, p is the pressure in kPa, and a,b, c and d are given by

$$a = A_1 + B_1 m_{Si}^{w} + C_1 (m_{Si}^{w})^2 + D_1 (m_{Si}^{w})^3$$

$$b = A_2 + B_2 m_{Si}^{w} + C_2 (m_{Si}^{w})^2 + D_2 (m_{Si}^{w})^3$$

$$c = A_3 + B_3 m_{Si}^{w} + C_3 (m_{Si}^{w})^2 + D_3 (m_{Si}^{w})^3$$

$$d = A_4 + B_4 m_{Si}^{w} + C_4 (m_{Si}^{w})^2 + D_4 (m_{Si}^{w})^3$$

where m_{Si}^{w} is the silica concentration in the water phase and the coefficients A_i to D_i are given in Table 3.4. The concentration of silica in vapor over water is shown is Figure 3.7 as a function of pressure and silica concentration in the water phase. As observed, the silica concentration in vapor decreases with decreasing pressure and silica concentration in the water phase.

3.5 Superheated vapor depressurization and condensation

The formation of superheated steam in the Krafla system is likely to be caused by heat in addition to geothermal water, followed by boiling to single phase superheated vapor. Non-volatile components including Na, K, Ca, Mg, Fe and Al are lost upon this boiling by mineral formation, leading to concentrations of <1 ppm in the vapor phase for these elements. Most of the silica in the geothermal water is also lost upon boiling; however, the silica solubility in the superheated vapor is significant or around ~10-150 ppm depending on pressure and assuming quartz solubility. The volatiles, including CO_2, H_2S, Cl, F and B, on the other hand, are preserved and enter into the superheated vapor phase.

Upon ascent to the surface, the superheated vapor depressurizes. The depressurization within a well like IDDP-1 is likely to be close to isoenthalpic. Because of the enthalpy, the pressure and temperature relationship in superheated steam at <600°C will also decrease at constant enthalpy with decreasing pressure within the superheated vapor region. The exact depressurization path of the superheated vapor (or in fact supercritical fluid at <500 bar), largely depends on the initial enthalpy of the vapor. If the initial enthalpy of the vapor is below the maximum enthalpy of vapor in the two-phase system (<2800 kJ/kg), the depressurization will lead to vapor condensation. This path is expressed in Figure 3.8 as A, B to C path. If the enthalpy of the superheated vapor is greater than the maximum

Table 3.4
Coefficients to calculate solubility of silica in vapor in two-phase systems (after Bahadori and Vuthaluru, 2010)

Coefficient	Coefficient for <50 ppm in water	Coefficient for 50-500 ppm in water
A_1	-9.91036274604	-7.297158278
B_1	3.60353241190E-01	3.36188512456E-02
C_1	-1.30855233907E-02	-1.20354059517E-04
D_1	1.50175517061E-04	1.29245662436E-07
A_2	4.09783293899E-04	4.18453241026E-04
B_2	1.57322016793E-05	5.55318691455E-08
C_2	-1.01366560040E-06	-1.70390526490E-09
D_2	1.38530459540E-08	5.40562939438E-12
A_3	2.37599942152E-09	2.78159673634E-09
B_3	-1.20699785241E-09	1.09878426400E-11
C_3	7.68541076834E-11	5.52027970387E-15
D_3	-1.01195964275E-12	-2.51031446555E-16
A_4	-4.79364161851E-14	-8.17515244627E-14
B_4	2.79052818094E-14	-6.16067430892E-16
C_4	-1.77452718145E-15	2.81610902151E-18
D_4	2.26671481870E-17	2.01005793400E-21

enthalpy of vapor in the two-phase field (>2800 kJ/kg) the depressurization occurs in the vapor only stability field. This path is expressed in Figure 3.8 as path D to E.

The geochemical consequences of the two paths are very different. In the case of vapor condensation, the fluids are enriched in the dissolved elements including F, Cl and B and the Si. Such condensed vapor (water) has a very low pH and may be chemically aggressive. Superheated or supercritical vapor condensation may be the cause of low pH fluids in some wells in Krafla, commonly referred to as acid wells. The vapor condensation was modelled assuming iosenthalpic conditions. In the example, the single phase vapor was assumed to have an initial temperature of 425°C and enthalpy of 2750 kJ/kg. The results are shown in Figure 3.9 and refer to the path in Figure 3.8 A-B-C. The fraction of condensed liquid is very small, or <0.03 (<3%) at all pressures. Assuming that non-volatile components enter quantitatively into the condensed vapor, the concentration of these elements in the condensate will be extremely high. On the other hand, the concentration of volatiles in the vapor phase is insignificantly affected by the formation of this small mass of vapor condensate. An example of the composition of condensed vapor and the associated vapor phase is given in Table 3.5 and further compared with IDDP-1 vapor, a sample collected from Krafla well 36 (Hauksson, 2008) and the Krafla geothermal water composition used earlier in the model calculation of IDDP-1 upon boiling. As observed, there are similarities between the modelled condensed vapor from superheated vapor, equilibrated Krafla geothermal

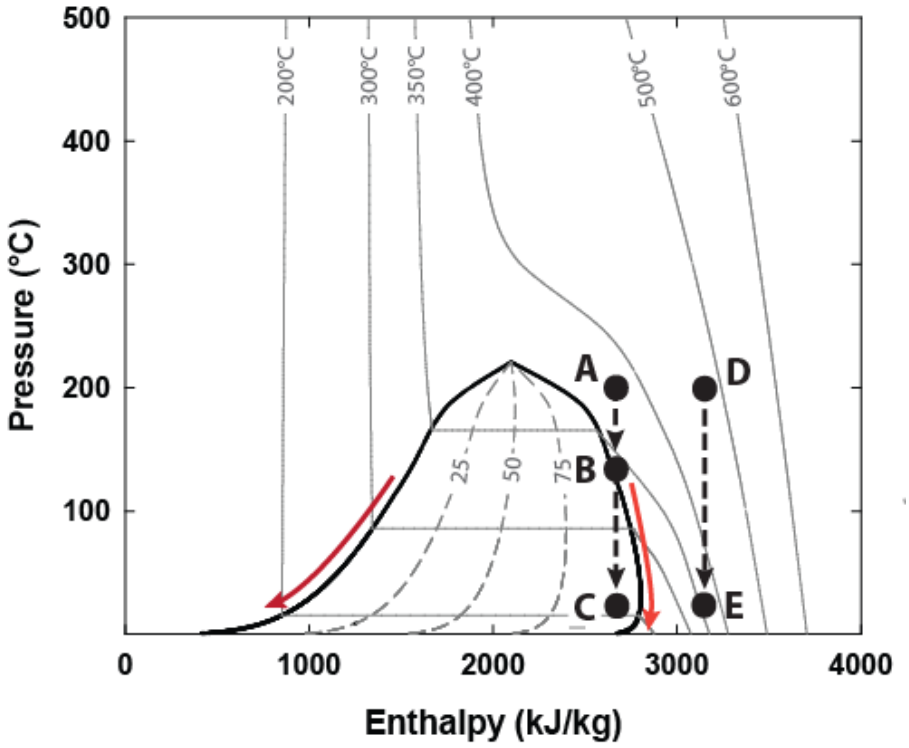

Figure 3.8. *The possible pathways of superheated vapor upon depressurization. Two scenarios are shown. Firstly, a superheated vapor (A) has a lower initial enthalpy than the maximum enthalpy of vapor in the two-phase region depressurizes. This vapor will hit the two-phase curve for H_2O followed by formation of a small mass of condensed vapor (B). Upon further depressurization, vapor and liquid water are formed (C), the fraction of vapor being >95% in most cases. Secondly, a superheated vapor (D) has a greater initial enthalpy than the maximum enthalpy of vapor in the two-phase region depressurizes. This vapor will depressuize without vapor condensation all the way up to the surface at 1 bar.*

water and the acid discharge from Krafla well 36. In fact, the acid water in Krafla well 36 mimics a mixture of condensed superheated vapor and geothermal water, pointing to a possible formation mechanism of such acid fluids in Krafla.

On the other hand, the depressurization of superheated vapor with high enthalpy will lead to no phase changes and vapor condensation. However, significant silica may be precipitated upon the depressurization as the solubility of silica in single phase vapor decreases sharply with decreasing pressure. The volatiles, CO_2, H_2S, Cl, F, B , however, are largely unaffected by depressurization of a single phase vapor. This is considered to be the case for IDDP-1.

3.6 Silica formation upon depressurization of superheated vapor

Silica formation may be an effective process during both boiling of geothermal water to superheated vapor and superheated vapor depressurization. The formation of other

Table 3.6
Mass of silica formation upon boiling of geothermal water and depressurization of superheated vapor assuming quartz solubility

	Discharge (kg/sec)			
	1	10	25	50
	Silica formation (kg/day SiO_2) at variable discharge			
Boiling at 265°C to dry steam at constant pressure	46	461	1151	2303
Depressurization of superheated vapor at 450°C and 3200 kJ to 150 bar	3	29	71	143
Depressurization of superheated vapor at 450°C and 3200 kJ to 100 bar	5	48	121	242
Depressurization of superheated vapor at 450°C and 3200 kJ to 50 bar	6	57	143	285
Depressurization of superheated vapor at 450°C and 3200 kJ to 10 bar	6	60	149	298
	Duration (days) to fill pore space of 1-m^3 rock with 40% porosity with silica at variable discharge [a]			
Boiling at 265°C to dry steam at constant pressure	23	2.3	0.9	0.5
Depressurization of superheated vapor at 450°C and 3200 kJ to 150 bar	373	37	15	7.5
Depressurization of superheated vapor at 450°C and 3200 kJ to 100 bar	220	22	8.8	4.4
Depressurization of superheated vapor at 450°C and 3200 kJ to 50 bar	187	19	7.5	3.7
Depressurization of superheated vapor at 450°C and 3200 kJ to 10 bar	178	18	7.1	3.6
	Duration (days) to fill 10-m long pipe with 20-cm diameter with silica at variable discharge [a]			
Boiling at 265°C to dry steam at constant pressure	18	1.8	0.73	0.36
Depressurization of superheated vapor at 450°C and 3200 kJ to 150 bar	293	29	12	5.9
Depressurization of superheated vapor at 450°C and 3200 kJ to 100 bar	173	17	6.9	3.5
Depressurization of superheated vapor at 450°C and 3200 kJ to 50 bar	146	15	5.9	2.9
Depressurization of superheated vapor at 450°C and 3200 kJ to 10 bar	140	14	5.6	2.8

[a] Calculated quartz density of 2.66 g/cm^3

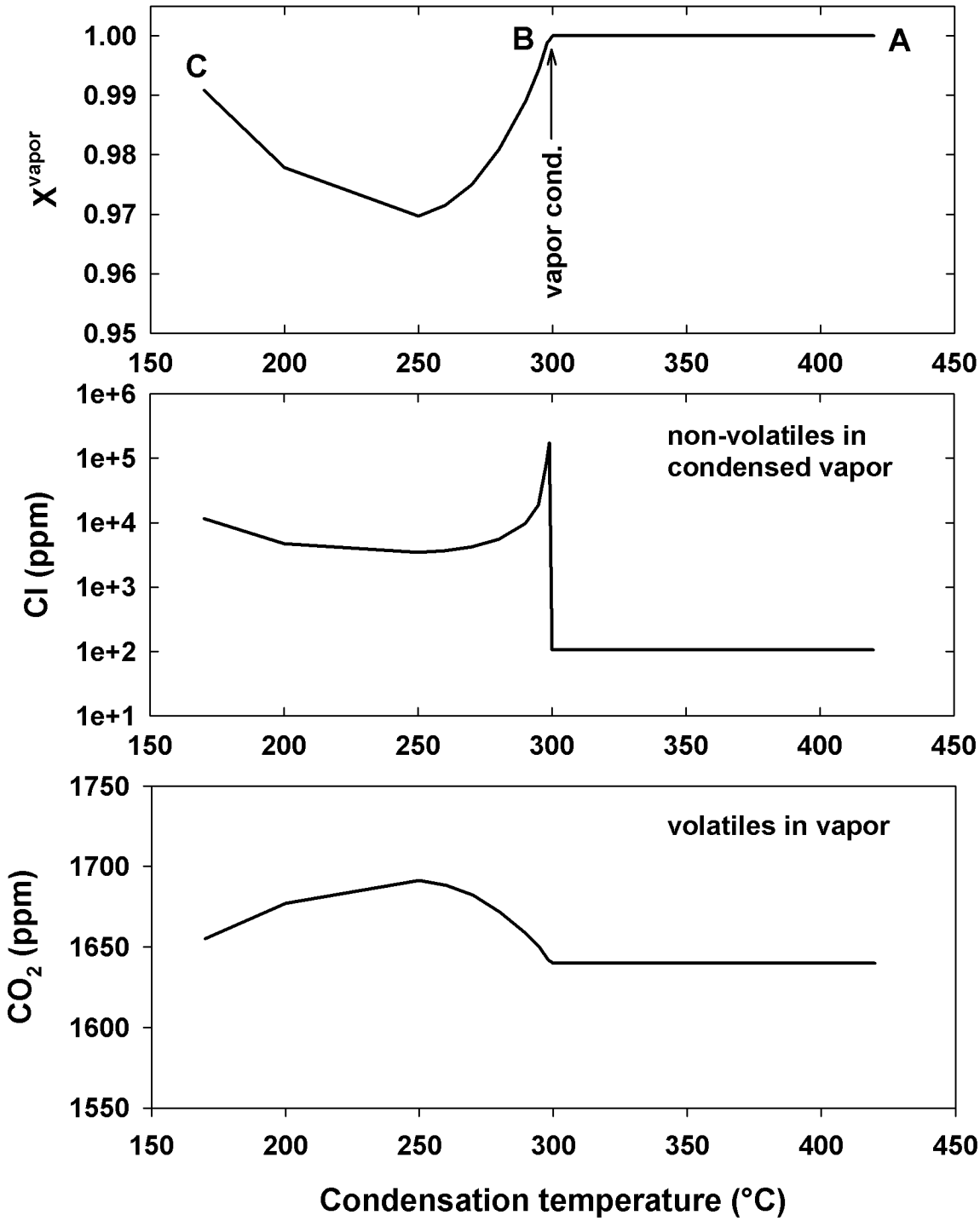

Figure 3.9. The chemical changes upon vapor condensation (Figure 3.8, path A-B-C). The vapor fraction (X^{vapor}), concentration of non-volatiles in condensed vapor (Cl as an example) and volatiles in vapor (CO_2 as an example) upon superheated vapor condensation. As indicated, the condensed vapor fraction is very small at all temperatures, with concentrations of non-volatiles being very high in the condensate. The volatiles in the vapor phase, however, are insignificantly affected.

secondary minerals seems to be less important, but may still be significant, in particular Na- and K-containing aluminum silicates.

In order to evaluate the possible mass formation of silica during these processes, mass balance calculations were performed, where the silica mass transfer was calculated assuming quartz solubility. The results are given in Table 3.6. Silica formation upon boiling of geothermal water to a single phase vapor is quantitative and large or 46 kg SiO_2/day at 1 kg/sec discharge. This corresponds to filling up 40% pore space of 1-m^3 rock within 23 days, possibly leading to a very rapid decrease in permeability in rocks of such producing aquifers. The silica formation for superheated vapor upon depressurization is approximately 10 times less. However, silica scaling in superheated vapor upon depressurization may still cause severe problems. In the case of the IDDP-1 well, taking the well discharge to be 50 kg/sec, and depressurization to <150, it will take only 3-6 days to fill up a 10-m long pipe with inner diameter of 20 cm.

The conclusion is that formation of superheated vapor by boiling and depressurization of superheated vapor will cause severe silica scaling problems. The formation of vapor may lead to low permeability of the producing aquifers with time and scaling problems in wells discharging superheated vapor will be massive unless well head pressures are kept almost equal to reservoir pressures.

4 Reinjection into IDDP-1

4.1 Composition and chemistry of reinjection water

Among possible options for enhancing thermal extraction and geothermal fluid output is re-injection into deeper parts of geothermal systems. In relation to this, the IDDP-1 well and similar wells could serve as reinjection wells instead of production wells. This may be a feasible option given the severe problems of energy utilization from superheated vapor discussed in section 3. The geochemistry associated with reinjection fluids is discussed in this section.

Possible fluids available at Krafla today for reinjection include waste water and non-thermal water. Their chemical composition is given in Table 4.1.

The waste water represents a typical boiled water with elevated concentrations of dissolved non-volatiles and depleted concentration of volatiles. The non-thermal water available in Krafla bears some signatures of geothermal input, yet the concentration of dissolved elements is generally low.

4.2 Geochemical effects of reinjection into the Krafla geothermal system

The geochemical processes that may occur upon reinjection of waste water and non-thermal water into the deeper part of the Krafla system (>2000 m) were investigated. Three major processes were studied, firstly, fluid-rock interaction of injection water with basalts as the reinjection water enters the aquifer at depth, secondly, possible mixing between reinjection water and existing aquifer geothermal water in the Krafla system, and thirdly, mixing of reinjection water with superheated vapor.

The geochemical modelling was carried out with the aid of the PHREEQC program (Parkhurst and Appelo, 1999). In the case of the fluid-rock interaction modelling, reaction path modelling was carried out at 200-300°C by dissolving basalt of known composition (Table 4.2) by the reinjection water, either waste water or non-thermal water (Table 4.1), and allowing common geothermal minerals when at equilibrium to precipitate. The minerals included in the calculations were quartz, clinochlore, daphnite, epidote, clinozoesite, prehnite, grossularite, wollastonite, low albite, microcline, wairakite, calcite, magnetite, pyrite, pyrrhotite, sulfur and anhydrite. Their respective solubilities are given in Table 2.5. Thermal effects associated with reinjection are a subject outside the scope of this report. However, the temperature rise of the geothermal fluids within the well is often limited at a high injection rate. For simplicity, the base temperature of reinjection water was assumed to be equal to the wellhead temperature (water temperature in Table 4.1) and the increase in temperature was assumed to occur within the aquifer.

The results of the fluid-rock interaction modelling are shown in Figure 4.1 in terms of mineral saturation as a function of reaction progress. As discussed in section 2, the

Table 4.1
Chemical composition of possible reinjection water into the IDDP-1 well

Tími	Waste water [a]	Non-thermal water [a]
Discharge	146.5	
t°C	124.5	15.6
pH/°C	9.48/21	7.74/21
SiO_2	572	50.8
B	1.05	0.043
Na	233	21.1
K	29.4	2.89
Ca	3.56	24.9
Mg	0.014	9.74
Al	1.37	0.003
Fe	0.017	0.100
Cl	59.1	3.50
F	1.11	0.163
CO_2	68.5	104
H_2S	31.2	0.023
SO_4	243	29.3

[a] From Landsvirkjun database

composition of the geothermal fluids in Krafla is considered to be controlled close to equilibrium between the fluids and the secondary minerals found in the systems and included in the geochemical models. The composition of the reinjection water, both the waste water and non-thermal water, is different from the equilibrated geothermal fluid composition. Therefore, when the reinjection water enters the aquifer at depth, fluid-rock interaction will occur between the surrounding rocks and the reinjection water and continue until equilibrium conditions are attained. The amount of rock needed to attain this equilibrium state is given by the reaction progress (ξ) here defined as the mole of basaltic rock dissolved per kg of fluid. As observed in Figure 4.1, insignificant basaltic rock dissolution or mass movement is needed in most cases to attain equilibrium between the reinjection water and the geothermal minerals that subsequently form, or ξ <0.1 (<15 g of basalt per kg of water). This is true both in case of waste water and non-thermal water interaction with the rocks at temperatures between 200 and 300°C. At these temperatures, such degree of water-rock interaction has been experimentally demonstrated to take place within hours (Gysi and Stefánsson, 2012a,b). The concentration of CO_2 and H_2S in the waste water and non-thermal water is low compared to the concentration in the aquifer fluids at depth. This results in a far from equilibrium concentration for CO_2 and H_2S for the reinjection water. In order to attain equilibrium CO_2 and H_2S need to be added to the system, either by injection or by a natural input like magma degassing or rock leaching. Hydrogen (H_2), on the other hand, attains equilibrium rapidly due to reduction of water to form H_2 under geothermal conditions.

Table 4.2
The chemical composition of basalt (Stapafell) used for the reaction path simulations.
(after Gysia and Stefánsson, 2012a)

SiO_2 (wt%)	48.29
Na_2O	2.01
K_2O	0.29
FeO	10.47
Al_2O_3	14.47
MgO	8.45
CaO	12.2
TiO_2	1.58
MnO	0.19
Total	97.95

The secondary mineralogy formed according to the geochemical modelling is shown in Figure 4.2 as a function of reaction progress. The results at 250°C were taken as an example. The secondary mineral formation was found to be relatively insensitive to temperature at 200-300°C but largely dependent on reaction progress. The minerals initially formed included prehnite, wollastonite and chlorite. With increasing basalt dissolution the secondary mineralogy became dominated, however, by quartz, epidote, albite, chlorite and minor microcline. Sulfides (pyrite and pyrrhotite) were also observed to form, but this largely depended on the redox state of the system that is difficult to model accurately and the results should therefore be taken with care. Carbonates were found to be undersaturated in all cases, resulting in no calcite formation.

Another way of looking at the geochemical changes occurring upon reinjection into the Krafla geothermal system and subsequent water-rock interaction and mixing is to compare the result of the geochemical models with the equilibrium conditions occurring in the system. The equilibrium fluid composition can be viewed as the geochemical base value of the system that varies with temperature. The result of the geochemical models where the reinjection water was reacted with basalt to form secondary minerals is compared with the equilibrium conditions in the Krafla system in Figures 4.3 and 4.4. The modeled fluid composition represents results after basalt dissolution corresponding to the reaction progress of 0.01 to 0.1 mole basalt per kg water (ξ = 0.01-0.1). According to the results seen in Figure 4.1, this reaction progress should represent the early attainment of equilibrium between secondary minerals and the fluid. The modelled composition compares reasonable well in some cases with the observed equilibrium composition but differs in others. The discrepancy is considered to be mainly caused by a much lower CO_2 and H_2S concentration for the equilibrated reinjection water compared with the geothermal water (Fig. 4.4). As CO_2 and H_2S are among the main acids in geothermal water, the pH of the modelled

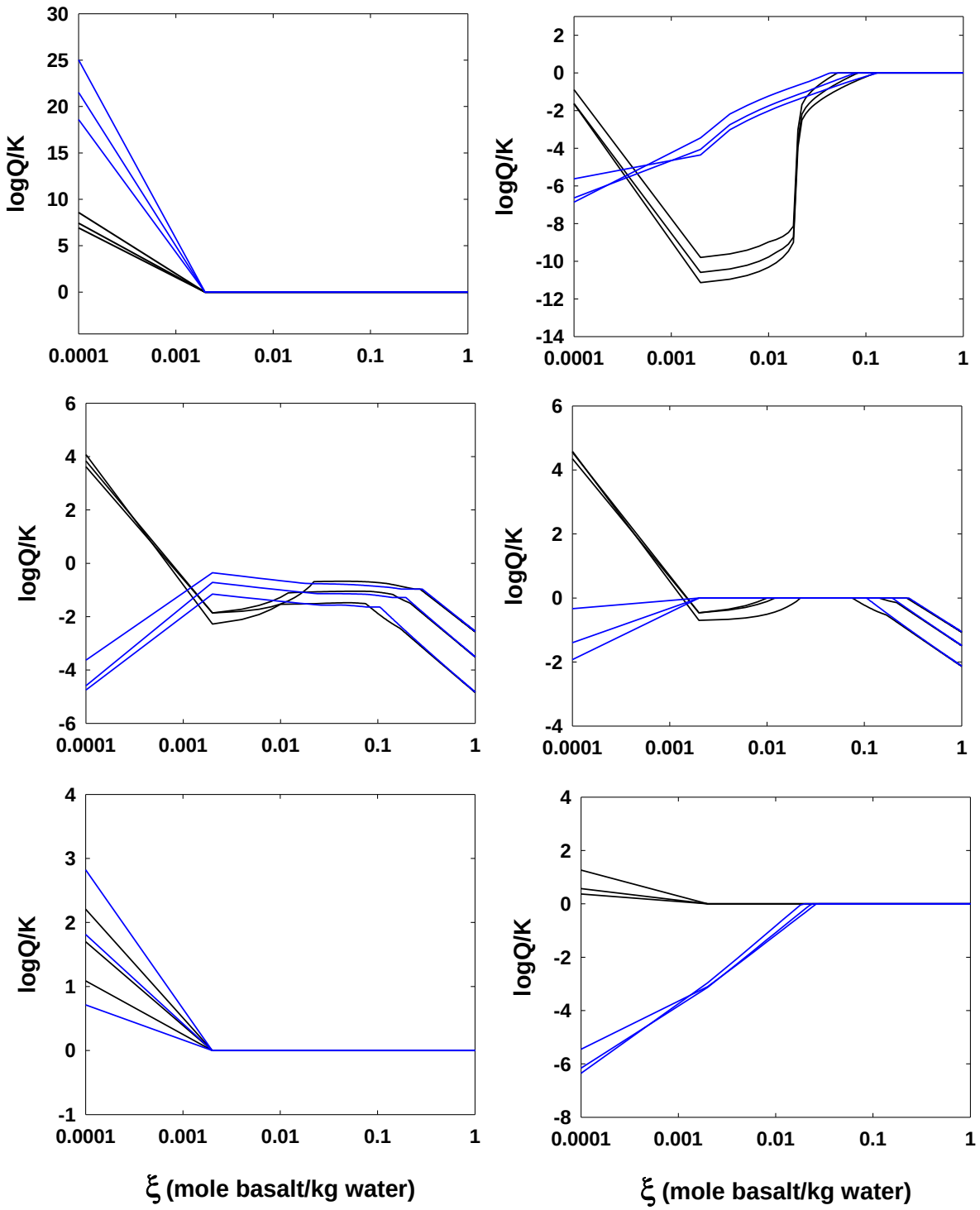
logQ/K
ξ (mole basalt/kg water)
0.0001
0.001
0.01
0.1
1

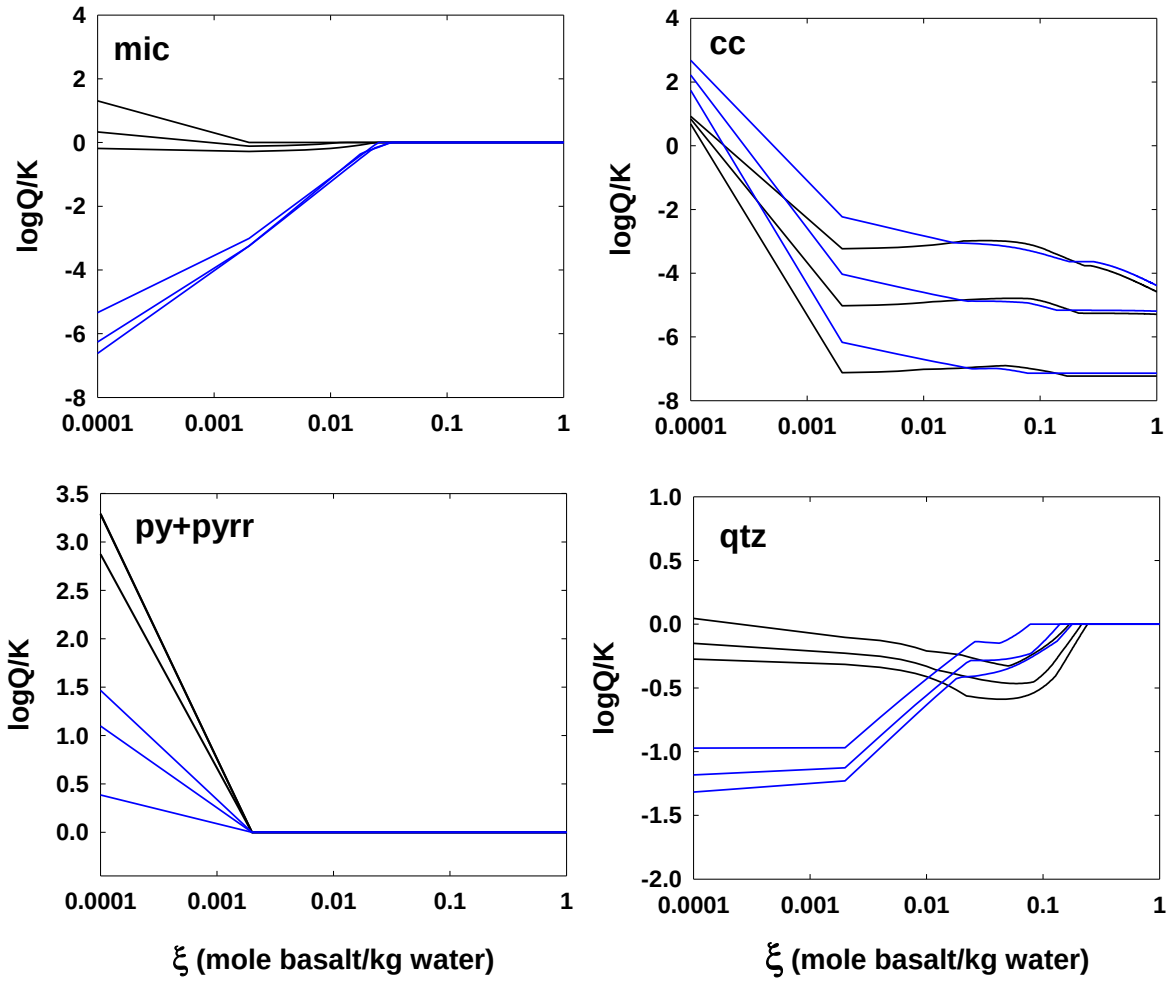

Figure 4.1. *Modelled mineral saturation (logQ/K) of reinjection water with basalt as a function of reaction progress (ξ). Equilibrium is attained when logQ/K = 0. The blue lines show the results for interaction between basalt and cold water at 200, 250 and 300°C and the black lines show interaction between basalt and geothermal waste water at 200, 250 and 300°C. The secondary minerals considered are those commonly observed within the Krafla geothermal system.*

reinjection water is higher (more alkaline) compared to the equilibrated geothermal water (Fig. 4.5). This in turn has important effects on aqueous speciation and mineral saturation

Possible mixing between the equilibrated reinjection water and the equilibrated geothermal water was also qualitatively assigned (Figs. 4.3 and 4.4). Mixing of reinjection water and equilibrated geothermal water will, in all cases, move the chemical composition of the reinjection water closer to the equilibrium composition of the geothermal water in Krafla. The mixing ratio, however, between equilibrated geothermal water and reinjection

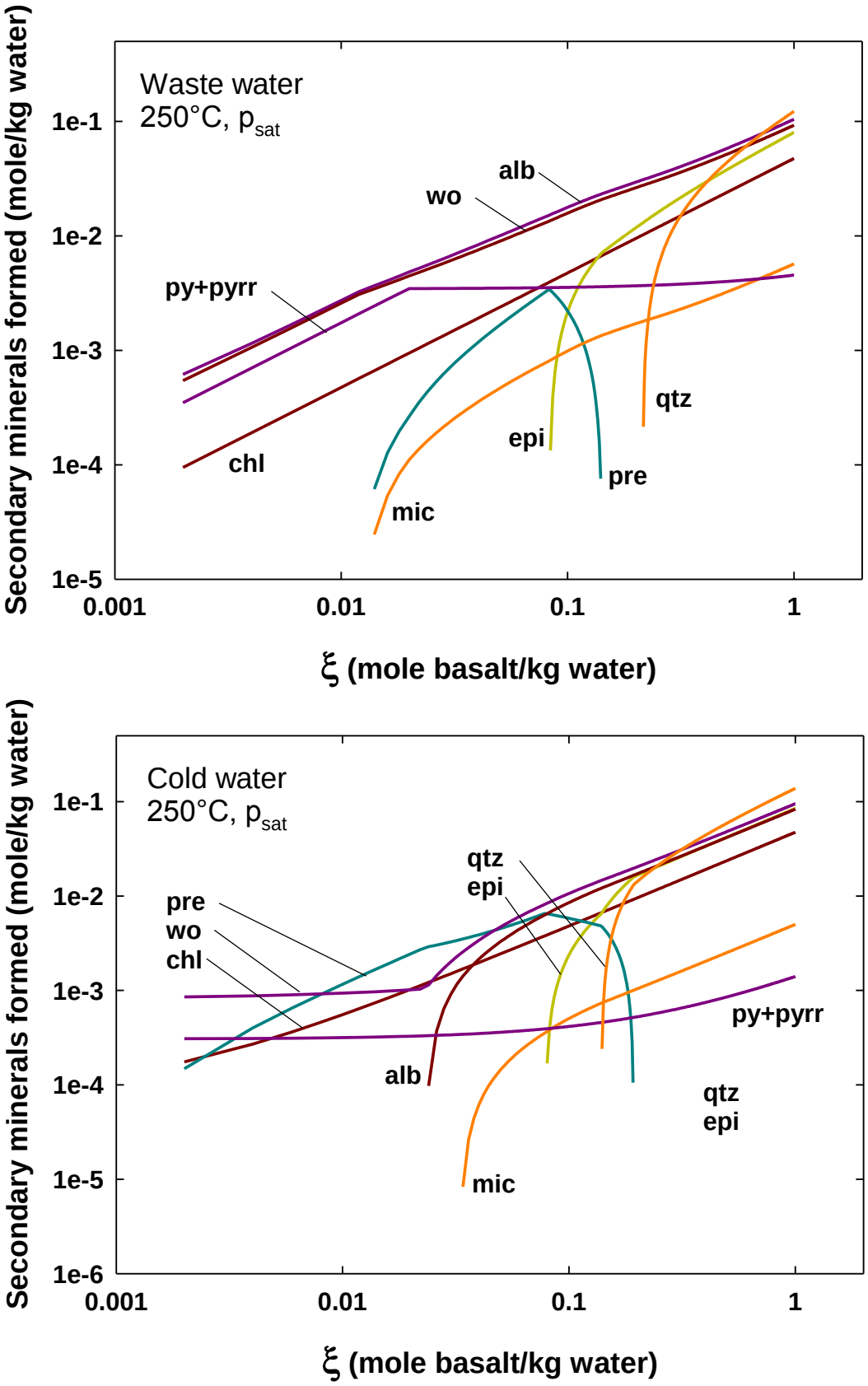

Figure 4.2. *Modelled secondary mineral formation upon interaction of reinjection water with basalt as a function of reaction progress (ξ) at 250°C.*

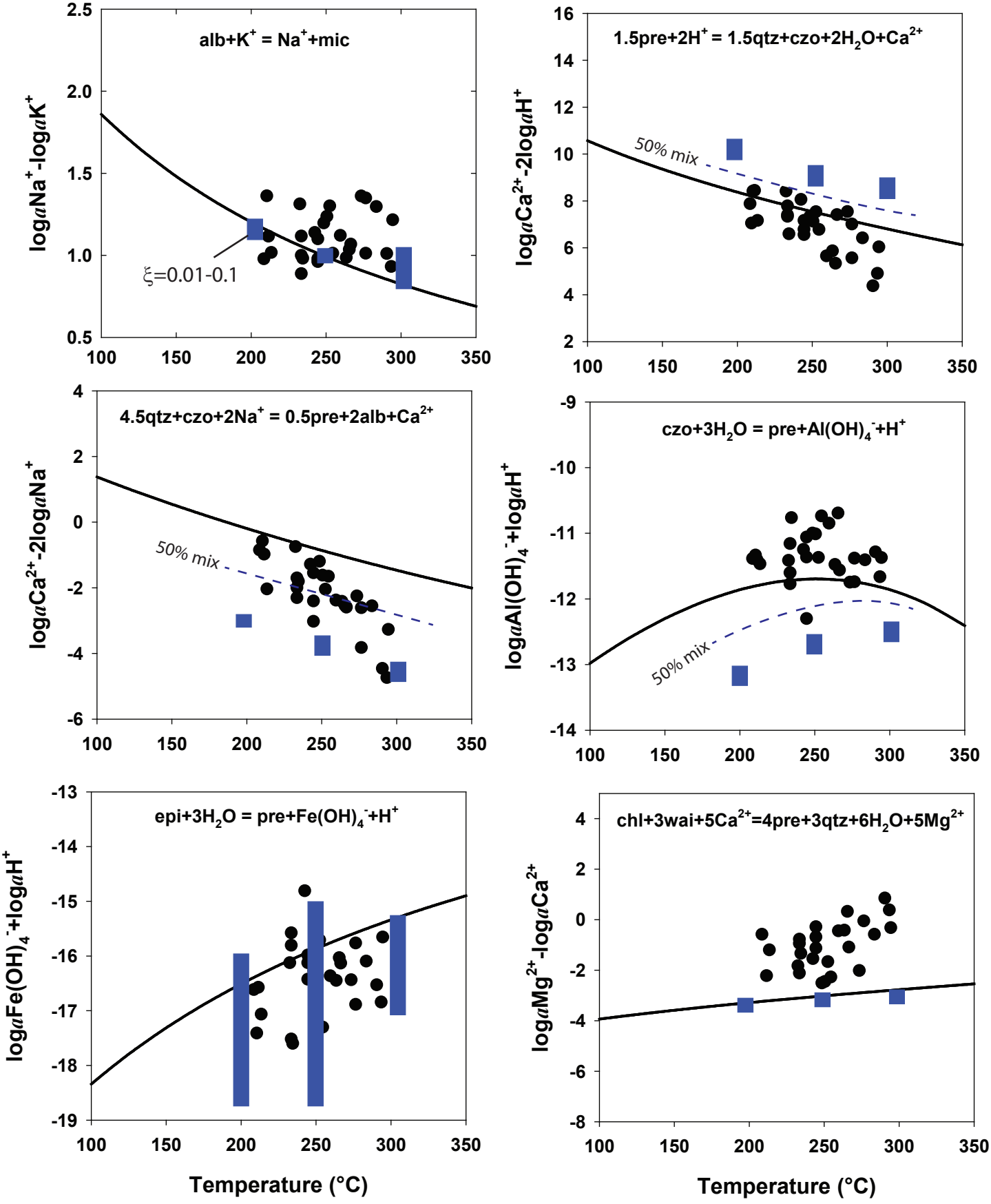

Figure 4.3. The comparison between the modelled composition of reinjection water after interaction with basalt (ξ= 0.01-0.1) (blue symbol), with calculated aquifer composition (section 2) (black dots) and the p roposed equilibrium conditions (black line). Also, shown are mixing lines between the reacted reinjection water with the proposed equilibrium conditions.

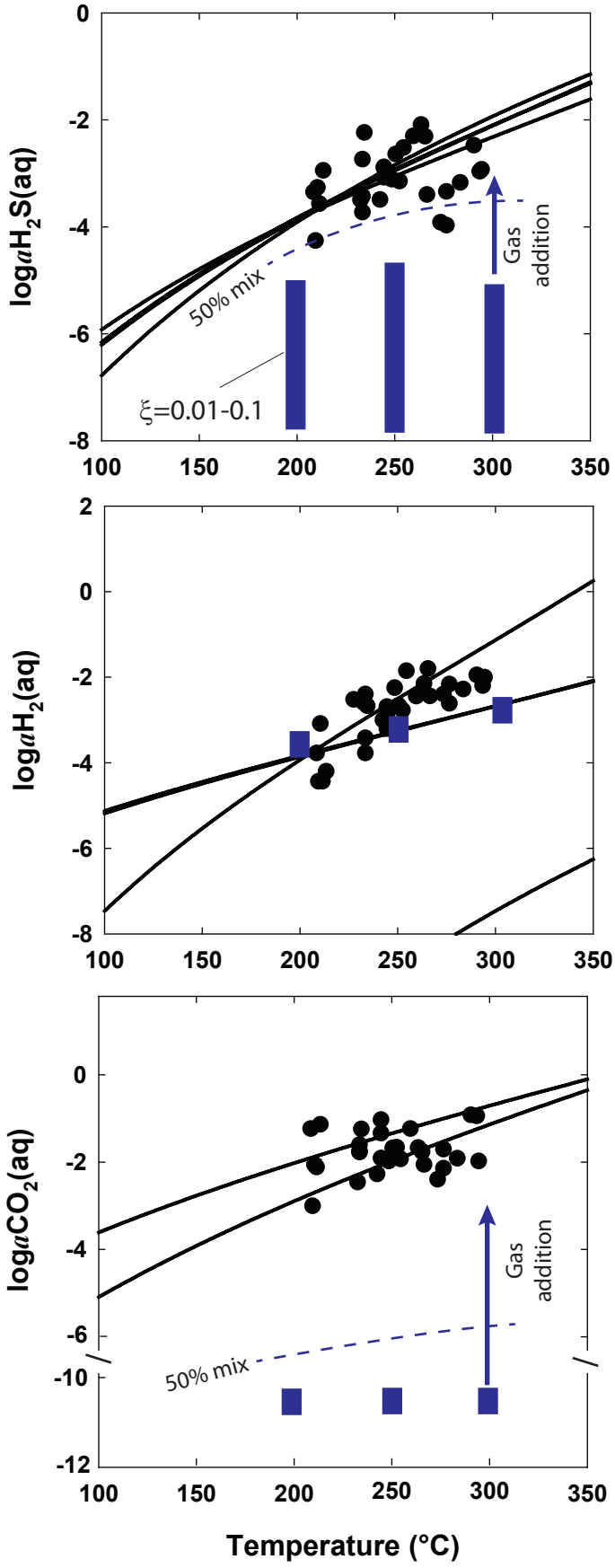

Figure 4.4. The variation of pH with temperature. The black dots show the results of aquifer pH calculated assuming liquid only in the the aquifer (model 1, see section 2), the line shows average pH of geothermal water in Iceland (Stefánsson and Arnórsson, 2002) and the blue boxes the modelled pH at 200, 250 and 300 of the reinjection water after reacting with basalt (ξ= 0.01-0.1).

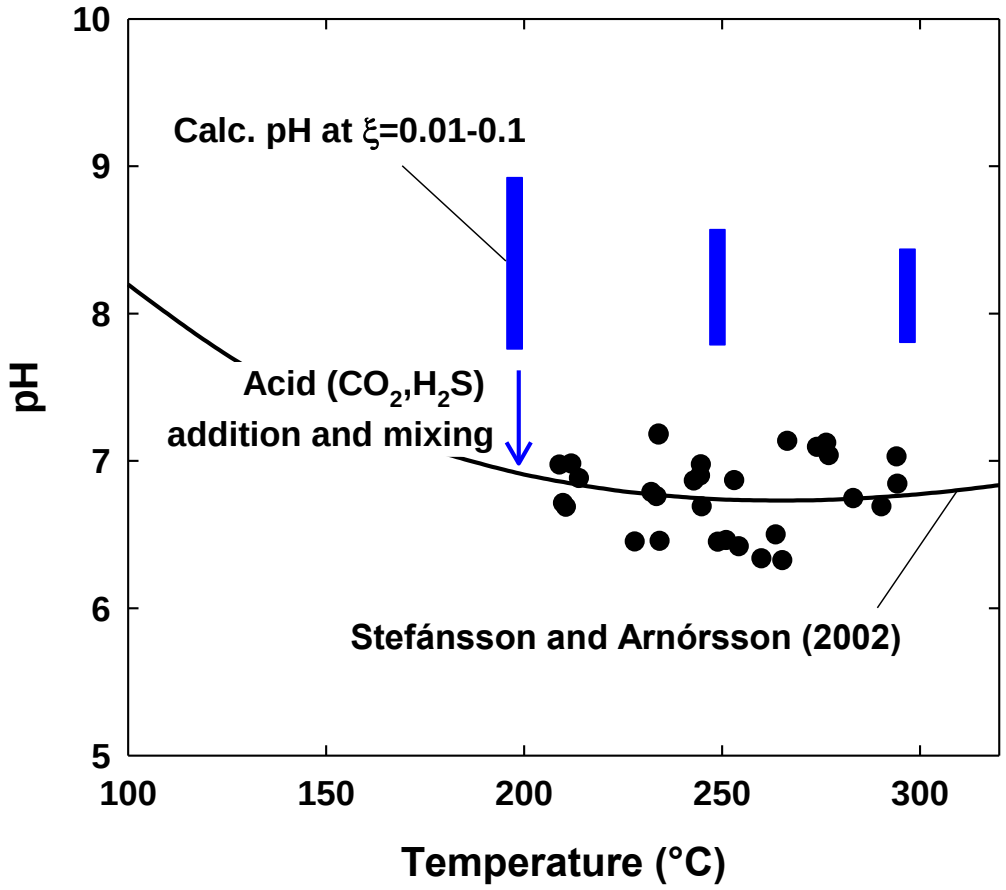

Figure 4.5. *Comparison between the modelled CO_2, H_2S and H_2 concentration of reinjection water after interaction with basalt (ξ = 0.01-0.1) (blue symbol), with calculated aquifer composition (section 2) (black dots) and the proposed equilibrium reaction (black lines). Also, shown are mixing lines between the reacted reinjection water with the proposed equilibrium reaction conditions.*

water needs to approach almost pure end-member equilibrium water composition to attain uniform composition within the aquifer.

The last model involved mixing of reinjection water with superheated vapor with an initial temperature of 450°C. A hypothetical mixing trend between reinjection water and superheated vapor is shown in Figure 4.6. The mixing will result in "vapor" boiling of the reinjection water within the two phase field with only pure superheated vapor existing as the ration of superheated vapor to reinjection water becomes >90% vapor. This indicates that superheated vapor will be condensed into reinjection water when the fraction of reinjection water in the mixture becomes more than 10%.

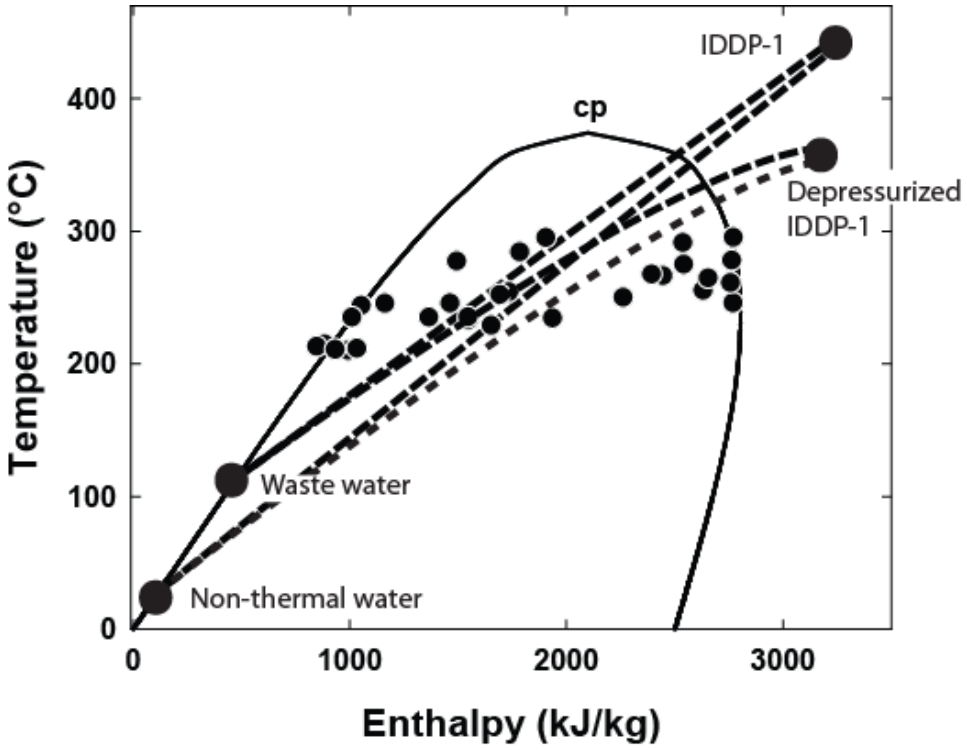

Figure 4.6. *The mixing trend between reinjection water and superheated vapor, IDDP-1 fluid at 450°C and depressurized IDDP-1 fluid to 100 bar having temperatures of 350°C.*

4.3 Possible geochemical signatures of reinjection

The possible natural geochemical signatures of reinjection within production wells may be difficult to assess without the addition of artificial tracers. Firstly, as discussed in section 4.3, a relatively minor reaction between the reinjection water and the basalt host rock is needed to attain close to equilibrium conditions of the aquifer fluids. It follows that most major elements including Si, Na, K, Ca, Mg, Al and Fe are inadequate as tracers of the proportion of reinjection water within production well discharges. The major differences may be related to CO_2 and H_2S concentrations. Assuming a limited supply of gaseous CO_2 and H_2S into the geothermal system, a significant input of reinjection water to the geothermal water may lead to decreased concentration. However, in the case of a gaseous supply of CO_2 and H_2S, for example through magma degassing, such decrease in gas concentration may not be observed.

Alternatively, non-reactive elements like Cl may be used as natural tracers for mixing as long as there is a significant difference in concentration between the reinjection water and the geothermal water. A potential mixing pattern between the two types of reinjection water and the geothermal water in Krafla is demonstrated in Figure 4.7. Mixing between the waste water and geothermal water has insignificant effects on Cl concentration, whereas

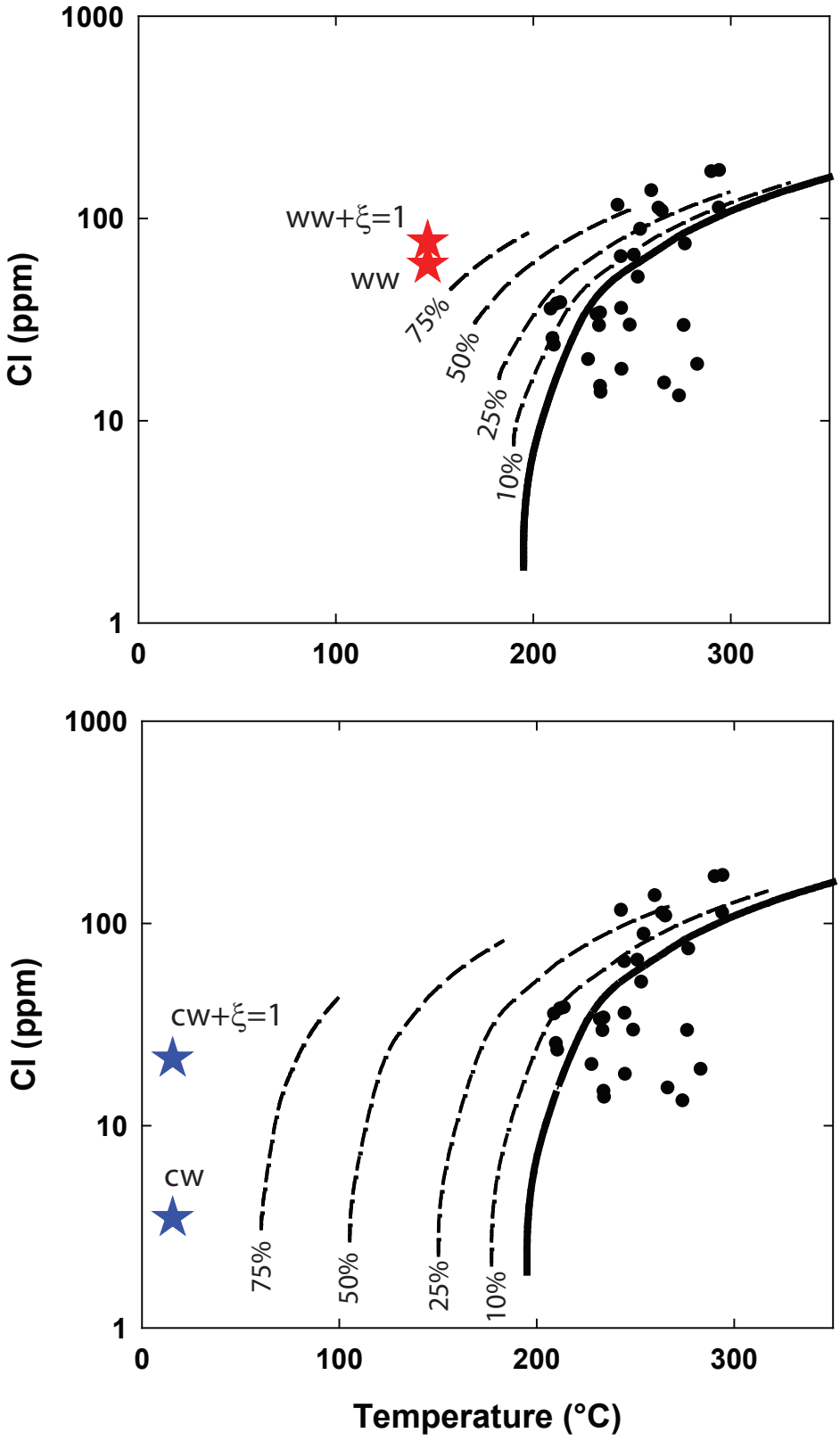

Figure 4.7. The relationship between temperature and chlorine concentrations. Dots represent the aquifer chlorine concentration in Krafla and the solid line shows the best fit through these data points. The red-star shows the composition of the waste-water reinjection ignoring thermal inputs and the blue start shows the composition of the non-thermal reinjection water. The dotted lines show various mixing ratios between the two. The effects of rock leaching are also demonstrated (ξ=1) taking the Cl concentration in basalt to be 150 ppm (Arnórsson and Andrésdóttir, 1995). As seen, rock leaching has very minor effects on the fluid composition.

temperature changes may be observed, ignoring heat input into the mixed fluid. On the other hand, significant Cl and temperature variations are observed in cases of non-thermal reinjection water mixing with geothermal water mixing.

Artificial tracers may also be used to trace mixing and flow patterns of the reinjection water. However, this may not be straightforward as trace amounts of common tracers may show reactive geochemical behavior within porous rocks under geothermal conditions (Moola et al., 2013). In addition, the thermal stability of many tracers within multicomponent geothermal fluid in contact with rocks is somewhat uncertain at present. Nonetheless, the use of artificial tracers in combination with non-reactive elements like Cl is probably the most feasible method for tracing mixing of reinjection fluids with equilibrated geothermal fluids. However, before such work is conducted it is important to perform tests under controlled conditions in the laboratory to evaluate the geochemical and thermal behavior of suitable tracers.

4.4 Consideration of the reinjection site

In this report, only the geochemical consequences of reinjection of waste water and non-thermal water to the deeper parts of the Krafla geothermal system were investigated. Here, it is shown that reinjection of relatively dilute water into high-temperature geothermal systems is geochemically feasible. Insignificant reactions are needed between the reinjection water and the host rock to attain close to equilibrium conditions of the existing geothermal fluids at temperatures above 200°C. Mixing will further help homogenize the system geochemically. However, the influence of hydrology, heat transfer and structural geology were not considered and it is very important when selecting a possible reinjection site to take all issues into account.

References

Anette K.M., Egilson Th., Árnadóttir S., Gautason B., Sigurgeirsson M. Á., Ingimarsdóttir A., Tryggvason H., Gunnarsson H. S., Jónsson R. B., Sveinbjörnsson S., Thorsteinsson E. (2010). Krafla IDDP-1. Drilling completion and geology report for drilling stage 3. Iceland GeoSurvey ÍSOR 2010/115. LV 2010/130.

Arnórsson S., Andrésdóttir A. (1995) Processes controlling the distribution of boron and chlorine in natural waters in Iceland. Geochim. Cosmochim. Acta 59, 4125–4146.

Arnórsson S., Angcoy E., Bjarnason J. Ö., Giroud N., Gunnarsson I., Kaasalainen H., Karingithi C. W., Stefánsson A. (2010) Gas chemistry of volcanic geothermal systems. World Geothermal Congress, Bali, Indonesia.

Arnórsson S., Bjarnason J.Ö., Giroud N., Gunnarsson I., Stefánsson A. (2006) Sampling and analysis of geothermal fluids. Geofluids 6, 203-216.

Arnórsson S., Gunnlaugsson E., Svavarsson H. (1983) The Chemistry of geothermal waters in Iceland 2. Mineral equilibria and independent variables controlling water Compositions. Geochim. Cosmochim. Acta 47, 547-566.

Arnórsson S., Sigurdsson S., Svavarsson H. (1982) The chemistry of geothermal waters in Iceland 1: Calculation of aqueous speciation from 0°C to 370°C. Geochim. Cosmochim. Acta 46, 1513-1532.

Arnórsson S., Stefánsson A. (1999) Assessment of feldspar solubility constants in water in the range 0° to 350°C at vapor saturation pressures. Amer. J. Sci. 299, 173-209.

Arnórsson S., Stefánsson A., Bjarnason J.Ö. (2007) Fluid-fluid interactions in geothermal systems. Rev. Min. Geochem. 65, 259-312.

Bahadori A., Vuthaluru H.B. (2010) Prediction of silica carry-over and solubility in steam of boilers using simple correlation. Applied Thermal Engineering 30, 250–253.

Benezeth P., Palmer D.A., Wesolowski D.J. (2001) Aqueous high-temperature solubility studies: II. The solubility of boehmite at 0.03 m ionic strength as a function of temperature and pH as determined by in situ measurements. Geochim. Cosmochim. Acta 65, 2097-2111.

Bjarnason J. Ö. (1994) The Speciation Program WATCH, Version 2.1. Reykjavik: National Energy Authority.

Diakonov I., Schott J., Martin F., Harrichourry J.-C. Escalier J. (1999) Iron (III) solubility and speciation in aqueous solutions. Experimental study and modeling. Part 1. Hematite solubility from 60 to 300°C in NaOH-NaCl solutions and thermodynamic properties of $Fe(OH)_4^-$(aq). Geochim. Cosmochim. Acta 63, 2247-2261.

Driesner T., Geiger S. (2007) Numerical simulation of multiphase fluid flow in hydrothermal systems. Rev. Min. Geochem. 65, 187-212.

Einarsson K., Pálsson B., Gudmundsson Á., Hólmgeirsson S., Ingason K., Matthíasson J., Hauksson T., Ármannsson H. (2010) Acid wells in the Krafla geothermal field. Proceedings World Geothermal Congress 2010.

Fournier R.O., Potter R.W. (1982) An equation correlating the solubility of quartz in water from 25 to 900°C at pressures up to 10 000 bars. Geochim. Cosmochim. Acta 46, 1969-1974.

Fridriksson T., Neuhoff P.S., Arnorsson S., Bird D.K. (2001) Geological constraints on the thermodynamic properties of the stilbite-stellerite solid solution in low-grade metabasalts. Geochim. Cosmochim. Acta 65 , 3993-4008.

Fridriksson Th., Gudfinsson G.H., Óskarsson F., Thorbjörnsson D. (2013) IDDP-1 flow test 2011 – chemical monitoring. *In* IDDP-1 Flow tests 2010-2012. Landsvirkjun LV-2013-050, 61-88.

Gautason B., Árnadóttir S., Mortensen A.K., Egilson Th., Gudfinnsson G. H., Sigurgeirsson M.Á., Jónsson R. B., Tryggvason H., Gunnarsson H. S., Sveinbjörnsson S., Thorsteinsson Th., Sveinbjörnsson S., Ingimarsdóttir A., Massiot C. (2010). Krafla – IDDP-1. Drilling completion and geology report for drilling stage 4. Iceland GeoSurvey ÍSOR 2010/116. Landsvirkjun LV 2010/131.

Gudmundsson B.T., Arnórsson S. (2005) Secondary mineral-fluid equilibria in the Krafla and Námafjall geothermal systems, Iceland. Appl. Geochem. 20, 1607-1625.

Gunnarsson I., Arnórsson S. (2000) Amorphous silica solubility and the thermodynamic properties of H_4SiO_4 in the range of 0° to 350°C at p_{sat}. Geochim. Cosmochim. Acta 64, 2295-2307.

Gysi A.P., Stefánsson A. (2012a) Experiments and geochemical modeling of CO_2 sequestration during hydrothermal basalt alteration. Chem. Geol. 306–307, 10–28.

Gysi A.P., Stefánsson A. (2012b) Mineralogical aspects of CO_2 sequestration during hydrothermal basalt alteration — An experimental study at 75 to 250 °C and elevated pCO_2. Chem. Geol. 306–307, 146-159.

Hayba D.O., Ingenbritsen S.E. (1997) Multiphase groundwater flow near cooling plutons. J. Geophys. Res. 102, 12235-12252.

Hauksson T. (2008) Krafla acid wells. Landsvirkjun.

Hauksson T., Markússon S.H. (2013a) Wet scrubbing of IDDP-1 steam – pilot test results. *In* IDDP-1 Flow tests 2010-2012. Landsvirkjun LV-2013-050, 119-170.

Hauksson T., Markússon S.H. (2013b) Silica in superheated steam of the IDDP-1 exploratory geothermal well in Krafla - Experimental study. Landsvirkjun 32 pp.

Hill P.G. (1990) A unified fundamental equation for the thermodynamic properties of H_2O. J. Phys. Chem. Ref. Data, 19, 1233-1274.

Holland T. J. B., Powell R. (1998) An internally consistent thermodynamic data set for phases of petrologic interest. J. Metamorphic Petrol., 16, 309-343.

Hólmgeirsson S., Guðmundsson Á., Pálsson B., Bóasson H.Á., Ingason K., Þórhallsson S. (2010). Drilling operations of the first Iceland deep drilling well (IDDP). World Geothermal Congress.

Johnson J.W., Oelkers E.H., Helgeson H.C. (1992) SUPCRT92. A software package for calculating the standard molal thermodynamic properties of minerals, gases, aqueous species, and reactions from 1 to 5000 bar and 0 to 1000°C. Computer. Geoscience 18, 899-947.

Kaasalainen H., Stefansson A. (2011) Chemical analysis of sulfur species in geothermal waters.Talanta 85, 1897-1903.

Kennedy G.C. (1950) A portion of the system silica–water. Econ. Geol. 45, 629–653.

Manning C.E. (1994) The solubility of quartz in H2O in the lower crust upper-mantle. Geochim. Cosmochim. Acta 58, 4831-4839.

Markússon S.H., Einarsson K., Pálsson P. (Eds) (2013) IDDP-1 flow tests 2010-2012. Landsvirkjun LV-2013-050.

Marshall W.L., Franck E.U. (1981) Ion product of water substance 0°-1000°C, 1-10,000 bars. New international formulation and its background. J. Phys. Chem. Ref. Data 10, 295-304.

Moola P., Sigfusson B., Stefansson A. (2013) Reactive transport of common hydrological tracers in porous media – an experimental study. Mineralogical Magazine 77, 1784.

Mortensen A.K., Gudmundsson Á., Steingrímsson B., Sigmundsson F., Axelsson G., Ármannsson H., Björnsson H., Ágústsson K., Sæmundsson K., Ólafsson M., Karlsdóttir R., Halldórsdóttir S., Hauksson T. (2009) Jarðhitakerfið í Kröflu - Samantekt rannsókna á jarðhitakerfinu og endurskoðað hugmyndalíkan. Iceland GeoSurvey ÍSOR-2009/057.

Neuhoff P.S. (2000) Thermodynamic properties and parageneses of rock-forming zeolites. Ph.D. Thesis, Stanford University, Stanford, CA, 240 pp.

Óskarsson F., Fridriksson Th. (2013) IDDP-1 flow test in 2012 – chemical monitoring. *In* IDDP-1 Flow tests 2010-2012. Landsvirkjun LV-2013-050, 89-115.

Parkhurst, D. L., Appelo, C. a. J. 1999. User's guide to PHREEQC (version 2)-A computer program for speciation, batch-reaction, one-dimensional transport, and inverse

geochemical calculations. Denver: U.S. Geological Survey Water-Resources Investigations Report 99-4259.

Rimstidt J.D. (1997) Quartz solubility at low temperatures Geochim. Cosmochim. Acta 61, 2553–2558.

Robie R. A., Hemingway B. S. (1995) Thermodynamic properties of minerals and related substances at 298.15 K and 1 bar (10^5 Pascals) pressure and higher temperatures. U. S. Geol. Surv. Bull. 1452, 436 p.

Scott S., Gunnarsson I., Arnórsson S., Stefánsson A. (2014) Gas chemistry, boiling and phase segregation in a geothermal system, Hellisheidi, Iceland. Geochim. Cosmochim. Acta 124, 170-189.

Stefánsson A., Arnórsson S. (2002) Gas pressures and redox reactions in geothermal fluids in Iceland. Chem. Geol. 190, 251-271.

Stefánsson A., Arnórsson S. (2000) Feldspar saturation state in natural waters. Geochim Cosmochim Acta 64, 2567-2584

Stefánsson A., Arnórsson S. (2002) Gas pressures and redox reactions in geothermal fluids in Iceland. Chem. Geol. 190, 251-271.

Stefánsson A., Arnórsson S., Gunnarsson I., Kaasalainen H. (2009) Sequestration of H_2S from Hellisheidi power platn – a geochemical stufy. Sci. Inst. Report RH-14-2009, 84 pp.

Stefánsson A., Gunnarsson I., Giroud N. (2007) New methods for the direct determination of dissolved inorganic, organic and total carbon in natural waters by Reagent-Free Ion Chromatography and inductively coupled plasma atomic emission spectrometry. Anal. Chim. Acta 582, 69-74.

Ziemniak S.E., Jones M.E., Combs K.E.S. (1995) Solubility behavior of titanium(IV) oxide in alkaline media at elevated temperatures. J. Sol. Chem. 22, 601-623.

Landsvirkjun

Háaleitisbraut 68
103 Reykjavik
landsvirkjun.is

landsvirkjun@lv.is
Sími: 515 90 00

Prentað efni